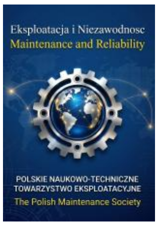

Eksploatacja i Niezawodnosc - Maintenance and Reliability

Volume 29 (2027), Issue 2

https://ein.org.pl

The Polish Maintenance Society

A health indicator-driven adaptive feature mode decomposition method for intelligent bearing fault diagnosis

Xingru Pan[1], Zhiling Peng[1,*]

[1] School of Mechanical and Electrical Engineering, North University of China, China
* Corresponding Author: pengzhilingnuc@163.com

Received: 11 May 2026
Revised: 3 July 2026
Accepted: 21 July 2026
Online: 4 September 2026

Abstract

This abstract describes a method for rolling bearing fault diagnosis. Mechanical equipment with rotating components often produces complex vibration signals where fault-induced periodic pulses are masked by noise and coupled together in compound fault scenarios, making diagnosis difficult. Although the original Feature Mode Decomposition (FMD) is applicable to analyse the non-stationary signals, its diagnostic performance is critically constrained by the empirical presetting of its key parameters, particularly the filter length (L) and mode number (n). To resolve this limitation inherent in conventional FMD, a parameter-adaptive framework, termed EPFMD, is developed. This approach systematically optimizes the key parameters to enhance decomposition performance. This method uses a novel composite health indicator (EPCHI) that combines envelope entropy (EE) and pulse factor (PF) as a fitness function. The EPCHI has the objective to accurately characterize fault features by measuring the pulse periodicity and the sparsity properties of the signal. The Ivy Algorithm (IVYA) is then employed to automatically optimize the parameter space. From the components decomposed by EPFMD, the most fault-sensitive component is selected using a fusion evaluation index (FEI) based on kurtosis and pulse factor. Finally, fault features are extracted via envelope demodulation. Tests on the CWRU dataset and experimental rigs show the method effectively diagnoses inner race, outer race, and compound bearing faults, outperforming other advanced techniques in comparisons.

Keywords: *composite health index, fusion evaluation index, adaptive feature mode decomposition, fault diagnosis, rolling bearing*

Article citation:
Pan X, Peng Z, A health indicator-driven adaptive feature mode decomposition method for intelligent bearing fault diagnosis, Eksploatacja i Niezawodnosc – Maintenance and Reliability 2027: 29(2) http://doi.org/10.17531/ein/231016

Highlights

- A parameter adaptive feature mode decomposition (EPFMD) method is proposed.
- The Ivy optimization algorithm (IVYA) has been utilised to make the FMD adaptive.
- A novel fusion index EPCHI is constructed to characterize the periodic impulses in signals.

1. Introduction

As core power transmission components in modern industry and mechanical equipment, rotating mechanisms such as bearings are widely applied in critical fields including energy generation, transportation, and precision manufacturing. These precision components, when subjected to prolonged extreme operating conditions (e.g., high-speed rotation, heavy loads, and temperature fluctuations), are prone to progressive degradation such as material fatigue and surface wear. Their failure mechanisms combine sudden breakdown characteristics and latent deterioration patterns, often leading to unplanned downtime events, which not only lead to substantial financial losses and production interruptions but also endanger personnel safety and may even trigger catastrophic accidents [1,2]. Within complex industrial systems, localized damage in critical power transmission components such as rolling bearings excites broadband vibration responses characterized by nonlinear and non-stationary properties. Such fault-induced signals are typically contaminated by multi-source interference coupling (e.g., background noise, load fluctuations, and transmission path attenuation) in engineering scenarios, where nonlinear dynamic features are often overwhelmed by strong noise, forming complex time-frequency modulation effects. Particularly for components like rolling bearings with typical contact mechanics, conventional time-frequency analysis methods struggle to effectively decouple composite modulation components, creating significant bottlenecks in extracting weak features related to faults. Therefore, there is an urgent need to advance deep mining technologies for bearing defect-sensitive features under high-noise backgrounds and com-prehensive fault signal, providing technical support for ensuring the safety of critical equipment [3].

In recent years, fault diagnosis methods have gradually evolved towards intelligent approaches, with primary research directions focusing on deep learning-based intelligent fault diagnosis methods for rolling bearing condition monitoring and signal processing- and physics-driven fault feature extraction methods. Deep learning can automatically learn complex nonlinear features in a data-driven manner, thereby reducing the reliance on prior experience in manual feature extraction. However, in practical applications, challenges such as insufficient annotated data, class imbalance, and domain shift remain. To address data scarcity, Dong et al. [4] proposed an entropy-oriented semisupervised dynamic prototype contrastive learning (ESDPCL) method, which improves feature discriminability by leveraging pseudo-label selection and dynamically updated prototypes, while enhancing intra- and inter-class separability through entropy-guided contrastive optimization. For cross-domain and unlabeled scenarios, Wang et al. [5] introduced a spatial-channel collaborative multi-scale graph interaction deep transfer learning (SCMGIDTL) framework. By integrating spatial-channel prototype extraction with multi-scale graph interaction, the method enables effective multi-source knowledge transfer and category-level domain alignment, significantly improving unsupervised diagnostic performance. Furthermore, Li et al. [6] developed a convolutional-transformer reinforcement learning framework (LiteDPER-CTQN), which formulates fault diagnosis as a sequential decision-making problem. The model combines transformer-based multi-scale feature extraction with a reinforcement learning strategy, achieving adaptive diagnosis under limited data while improving interpretability through Q-value estimation.

Despite the remarkable progress of AI methods in fault pattern recognition, their performance often depends on a large amount of high-quality training data and strong consistency in data distribution. In real industrial scenarios, due to factors such as varying working conditions, noise interference, and compound fault coupling, training data often fail to adequately cover all operating states, leading to reduced model generalization. Moreover, deep learning models usually lack clear physical interpretability, and their training process involves high computational costs, requiring substantial hardware resources and large-scale data. Therefore, under complex conditions and with limited samples, fault feature extraction methods driven by signal processing and physical mechanisms remain of significant research value. This technology has established a complete system for bearing fault diagnosis, making it the most universally applicable solution in rotating machinery condition monitoring. Examples include empirical wavelet transform (EWT), short-time Fourier transform (STFT), and generalized S-transform (GST) [7]. However, traditional time-frequency analysis methods for non-stationary signals suffer from inherent limitations such as strong dependency on parameter presets and sensitivity to window/base function matching. To overcome these challenges, adaptive decomposition theories based on signal intrinsic characteristics have emerged, innovatively constructing dynamic decomposition frameworks that autonomously decouple multi-component signals without manual preset basis functions. These methods address the challenge of transient impact extraction in complex modulated signals by establishing adaptive separation models for nonlinear coupled vibration components. They are particularly effective for enhancing weak fault feature extraction in rotating machinery under strong background noise, offering new technical pathways for industrial and mechanical fault diagnosis [8]. Such intelligent processing methods overcome the rigidity of fixed parameters in traditional algorithms, enabling dynamic adjustment of analysis parameters to efficiently extract fault features across time-frequency domains, thereby providing more efficient and precise solutions for monitoring equipment under complex operating conditions. Well-known adaptive signal processing algorithms include local mean decomposition (LMD), empirical mode decomposition (EMD), variational mode decomposition (VMD), ensemble EMD (EEMD), successive VMD (SVMD), and symplectic geometry mode decomposition (SGMD) [9],

In rolling bearing fault diagnosis research, adaptive signal processing technologies have achieved multi-dimensional engineering applications through continuous technical evolution. Representative studies include: In the work of Chennana et al. [10], Minimum Entropy Deconvolution Adjustment (MEDA) was combined with Empirical Mode Decomposition (EMD) to improve the extraction of fault signatures in rolling bearing diagnosis. The method includes decomposing vibration signals into a series of IMFs with EMD and reconstructing the signals using MEDA to improve the detection of impulses from faults. Xu et al. [11] innovatively proposed an LMD-based fault feature enhancement framework. They decoupled vibration signals adaptively via LMD, constructed multi-scale sample entropy feature matrices to quantify complexity differences across fault states, and validated the method's feasibility through a least squares support vector machine (LS-SVM) decision fusion model trained with cross-validation. Liu et al. [12] introduced an SGMD-based multi-index fusion fault diagnosis method. The approach decomposes vibration signals into symplectic geometry components (SGCs) via SGMD, proposes a composite weighting model incorporating Pearson correlation coefficient (PCC), cosine difference factor (CDF), and variable entropy for adaptive reconstruction of key components, designs a power spectral entropy-weighted singular value construction method to form highly representative feature vectors, and establishes an ant colony optimization–enhanced extreme learning machine classification model. Simulations and experiments confirm the method's superior feature characterization capabilities.

Studies indicate that variational mode decomposition (VMD) decomposes signals into independent intrinsic modes via Wiener filter banks under a variational constraint framework. Its non-recursive decomposition mechanism and global optimization properties effectively suppress modal aliasing. Compared to wavelet transform (requiring basis function presets) and EMD-like methods (prone to recursive error accumulation), VMD demonstrates superior time-frequency energy concentration for early weak bearing fault detection, enabling precise separation of fault-induced impacts [13]. In recent years, to improve fault feature extraction under strong noise and intense periodic interference, researchers have proposed various band-pass filter (BPF) design methods based on dynamic models or finite element simulations. Such methods typically obtain the natural or resonance frequency bands of mechanical structures through finite element modal analysis and use them as the center frequencies of the band-pass filters, thereby achieving accurate extraction of fault-related resonance bands. Wang et al. [14] proposed a BPF design method based on finite element simulation, which identifies potential carrier frequencies through modal analysis and constructs BPFs with fixed bandwidths to enhance the ability of Minimum Entropy Deconvolution (MED) in extracting weak fault impulses from axial piston pump bearings. Subsequently, to overcome the reliance on empirical settings for fixed bandwidths, they further introduced a bandwidth optimization strategy based on a comprehensive kurtosis index, enabling adaptive optimization of BPF bandwidth and improving fault feature extraction performance under strong periodic interference. Furthermore, Guo et al. [15] proposed the simulation-driven difference mode decomposition (SDMD) method, which uses a finite element model to assist in constructing an optimal filter for out-of-band noise suppression. Combined with convex optimization to further suppress in-band noise, this method enhances fault diagnosis capability under strong periodic impact conditions. Li et al. [16,17] proposed the simulation-guided BCSMD method, which obtains the first bending modal frequency through finite element modal analysis and uses it as the center frequency for the initial filter in blind deconvolution, effectively preventing the algorithm from converging to non-fault frequency bands and improving the extraction of fault features in wind turbine bearings under strong periodic interference.

The above studies show that BPF designs assisted by dynamic models can effectively enhance weak periodic impulse features, especially in environments with strong noise and periodic interference. However, such methods usually depend on relatively accurate finite element models, material parameters, and boundary conditions. The modeling process is complex, and under variable operating conditions, speed fluctuations, or changes in structural parameters, modal frequencies may shift, affecting filter design accuracy. Moreover, in most of these methods, the center frequency and bandwidth of the filter are still determined in a fixed or semi-empirical manner, making it difficult to adaptively track complex non-stationary signals. In contrast, Feature Mode Decomposition (FMD) [18] adopts an adaptive iterative optimization mechanism based on a finite impulse response (FIR) filter bank. Driven by feature indicators such as Correlated Kurtosis (CK), it updates the filter coefficients so that the filter frequency band automatically converges to the fault impulse feature band. Unlike fixed BPF designs based on finite element simulations, FMD does not require building complex dynamic models or rely on pre-determined resonance bands. Instead, it achieves frequency band adjustment through a data-driven approach, offering better robustness and engineering applicability under complex operating conditions, variable speeds, and compound faults. Additionally, FMD can adaptively separate different fault feature bands through multi-mode iterative decomposition, demonstrating strong advantages in compound fault diagnosis. However, its engineering applications still face significant challenges: 1) Parameter sensitivity: The setting of decomposition mode numbers lacks quantitative criteria. Deviations from actual physical modes may induce modal aliasing, dispersing the energy of fault impact components; 2) Filter length selection directly affects frequency band resolution. Suboptimal parameters cause envelope spectrum sideband energy attenuation, severely impairing early weak fault identification accuracy. Most critically, existing evaluation metrics inadequately characterize decomposition quality, and traditional single-index optimization strategies carry high misjudgment risks under strong noise or comprehensive faults. Thus, optimizing FMD's two key parameters to enhance its fault feature extraction capability under strong noise and comprehensive faults has become imperative, with health indicator selection being central to parameter optimization. To address these issues, this study proposes the following contributions:

1) This study proposes an automatic parameter optimization method for FMD to bolster its adaptability to fault characteristics and enhance the extraction of bearing defect features. The IVYA is employed as the optimization core to achieve this objective
2) A novel Composite Health Index (CHI), designated as EPCHI, is established by integrating EE and PF to serve as the fitness function for the optimization algorithm. The EE quantifies signal sparsity through the energy distribution of the signal envelope, while the PF characteriz-es the impulsive nature of vibration signals. Furthermore, a Fusion Evaluation Index (FEI) is formulated, where the component with the highest FEI value is identified as the optimal mode from the decomposition results.
3) Comprehensive multi-case validations and comparative studies were conducted, followed by quantitative analysis, demonstrating the superiority and effectiveness of the proposed fault diagnosis methodology for rolling bearings.

The subsequent content of this research is arranged as follows. Section 2 presents the specific procedures of the FMD method and constructs a comprehensive evaluation indica-tor for selecting the dominant modes. And then Section 3 describes the deployment of the IVYA for optimizing FMD parameters, facilitating their adaptive tuning to fault signals. It also provides a thorough description of the construction methodology for the composite health indicator. An over-view of the technical workflow of the FMD with adaptive parameter selection method is given in Section 4. (referred to as EPFMD, the EPCHI-based FMD with adaptive parameter selection method). The robustness and effectiveness of the proposed methodology are rigorously evaluated in Section 5. This evaluation is conducted through detailed case studies and a series of comparative experiments with existing ad-vanced methods, supported by quantitative analyses using multiple metrics to enhance the method's validity and supe-riority. Section 6 concludes the work.

2. Basic theory

2.1. FMD procedure

FMD serves as a non-recursive signal decomposition framework designed for analyzing non-stationary signals. The technical foundation of this approach involves the construction of an adaptive FIR filter bank under frequency sub-band energy constraints, coupled with a dynamic mode sieving mechanism for optimal filter selection. Compared to traditional recursive modal decomposition methods (e.g., EMD), FMD overcomes error propagation caused by recursive operations through linear filter design and coefficient regeneration strategies, achieving high-precision modal separation while controlling accumulation of errors. Based on the FMD framework proposed by Miao et al. [18], the specific implementation procedure is as follows:

Step 1: Load the original signal x and input predefined parameters: filter length L, segmentation number K, and decomposition mode number n.

Step 2: Construct the FIR filter bank with K Hanning windows and assign the initial value of the iteration counter i as 1.

Step 3: Iterate using the formula $r_k^i = x * h_k^i$to obtain the filtered modal component signals (k=1, 2, …, K), where "*" denotes the convolution operation.

Step 4: Update the filter coefficients using the original signal x, decomposed modal components r_k^i, and the estimated fault period T_k^i. Here, T_k^i is derived from the maximum point of the autocorrelation spectrum subsequent to the zero crossing. Complete one iteration and set i=i+1.

Step 5: Determine whether i has reached the specified number of iterations; if not, repeat Step 3, otherwise move to Step 6.

Step 6: Calculate the correlation coefficient between every pair of modes to construct a $K \times K$ correlation coefficient matrix $CC_{(K\times K)}$. Select the two modes with the highest correlation coefficient and discard the mode with the smaller correlation kurtosis. Set K=K−1.

Step 7: Checks if the current number of modes Khas reached the predefined target n. If not, it loops back to Step 3 to continue the iterative process of decomposition and mode selection. Once K equals n, the iteration terminates, and the current n modal components are output as the final result.

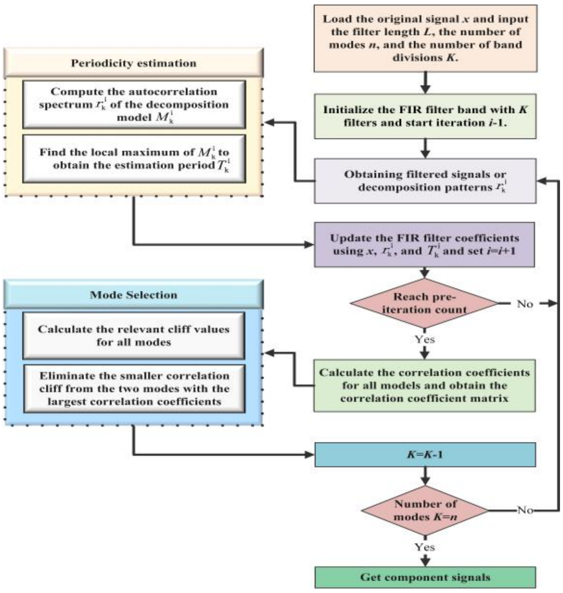

Figure 1. Flowchart of FMD method.

Fig. 1 presents the computational flowchart outlining the step-by-step procedure of the FMD algorithm.

2.2. Dominant mode selection criterion

In fault signal analysis, raw signals are often contaminated by complex noise sources such as mains-borne power-frequency interference and High-frequency stochastic noisy, leading to two critical challenges during signal decomposition: some decomposed modes (e.g., IMF components) may primarily represent noise energy with negligible correlation to fault characteristics; excessive redundant modes may be generated, where multiple components exhibit similar spectral properties or redundantly represent minor interference. Research indicates that the vibrational energy associated with genuine bearing faults is typically concentrated within a limited number of core Intrinsic Mode Functions (IMFs), often just 2 to 3 modes. Consequently, performing a quantitative evaluation of the relationship between the obtained modes and fault characteristics allows for the selection of a dominant mode that contain the most significant fault-related information. This process of mode selection effectively isolates fault signatures from background noise and redundant components, serving as an efficient data dimensionality reduction strategy. By focusing computational analysis on these most relevant modes, the method enhances the accuracy of feature extraction for precise fault identification while simultaneously minimizing the computational complexity and burden of subsequent diagnostic procedures

To address this, this section proposes a fusion evaluation index (FEI) combining frequency spectrum entropy (FSE) and kurtosis (K) serving as the criterion to identify the optimal mode. FSE evaluates the global complexity of spectral energy distribution. A higher FSE indicates more dispersed frequency components and greater spectral complexity. FSE is mathematically defined as [19]:

$$FSE = -\sum_{k=1}^{N} \frac{|X_k|^2}{\sum_{k=1}^{N} |X_k|^2} log_2 \left(\frac{|X_k|^2}{\sum_{k=1}^{N} |X_k|^2} + \epsilon \right) \tag{1}$$

Here, x represents the decomposed time series of length N. By applying the fast fourier transform (FFT) to x, the frequency spectrum X_k is generated:

$$X_k = \text{FFT}(x)[k], k = 1,2,\ldots,N \tag{2}$$

Kurtosis exhibits strong noise resistance while effectively capturing transient impacts in fault signals [20]. Its mathematical expression is given by:

$$K = \frac{\frac{1}{N}\sum_{i=1}^{N}(x_i-\bar{x})^4}{\left(\frac{1}{N}\sum_{i=1}^{N}(x_i-\bar{x})^2\right)^2} \tag{3}$$

where x_i denotes the i-th data point in the signal, $\bar{x}$ is the mean value, and N is the signal length.

In summary, Eq. 4 is defined as a comprehensive evaluation index for dominant mode selection. This criterion enables the identification of the optimal mode with the most prominent defect features from the decomposed sub-modes.

$$FEI = \frac{K}{FSE} \tag{4}$$

To validate the effectiveness of the proposed Fault Energy Index (FEI) in characterizing bearing fault features, four types of simulated signals were constructed: a single impulse (Signal 1), a harmonic signal (Signal 2), Gaussian white noise (Signal 3), and a periodic impulse signal (Signal 4), as illustrated in Fig. 2. The FEI was then compared with five representative indicators—namely, envelope entropy, pulse factor, kurtosis, average envelope entropy, and frequency spectrum entropy—by applying them to the four simulated signals. The calculated results of these indicators are presented in Fig. 3.

As shown in Fig. 3, the FEI exhibits higher sensitivity to periodic impulses excited by bearing faults compared to envelope entropy, pulse factor, kurtosis, average envelope entropy, and frequency spectrum entropy. Moreover, the normalized amplitude of the FEI remains lower than that of the other indicators when processing the three types of interference signals, namely harmonic, Gaussian white noise, and single impulse. This indicates that the FEI is less affected by single impulse, harmonic, and Gaussian white noise interference compared to the other indicators. In summary, the proposed FEI demonstrates stronger anti-interference capability and is more suitable for characterizing bearing fault-related information.

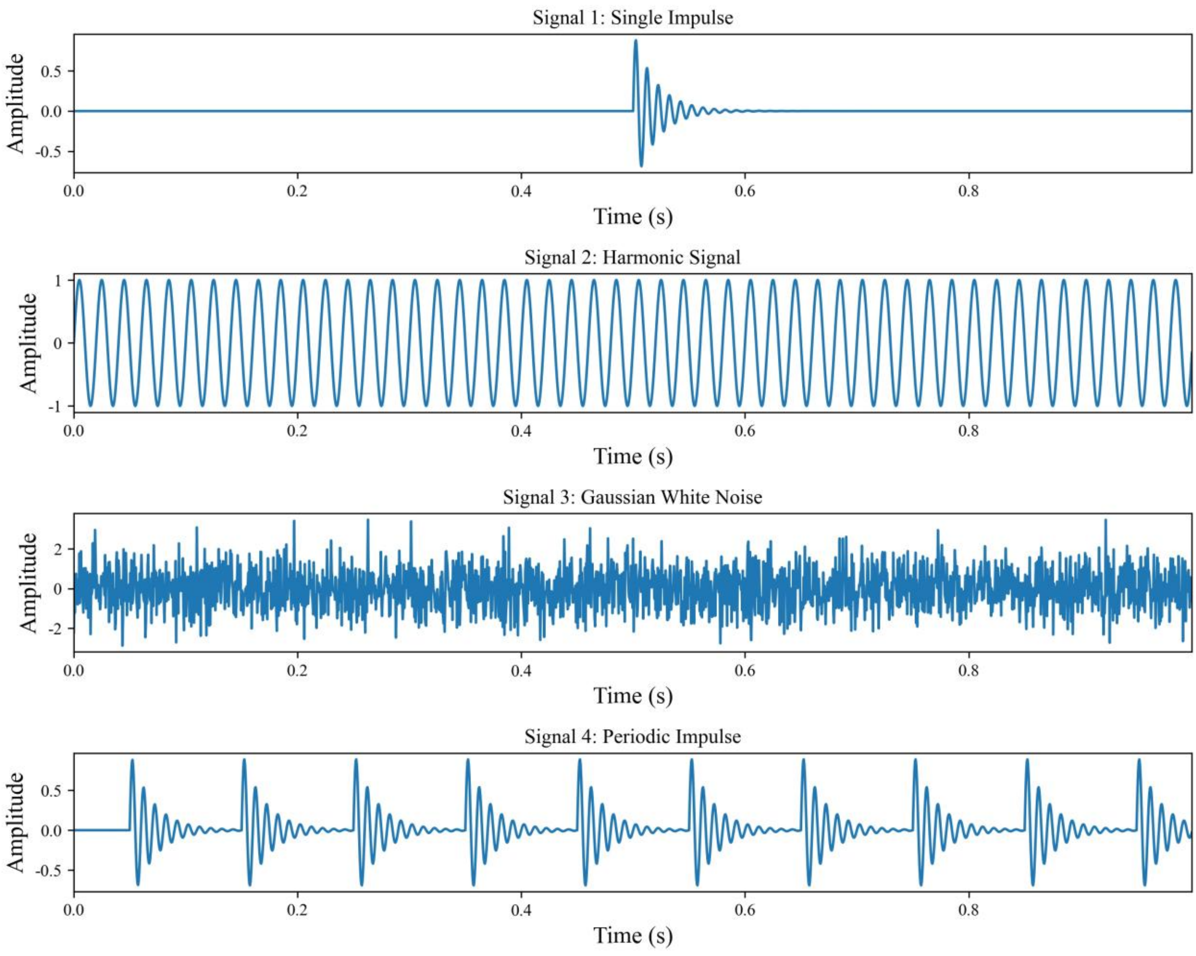

Figure 2. The time domain waveform of different signals.

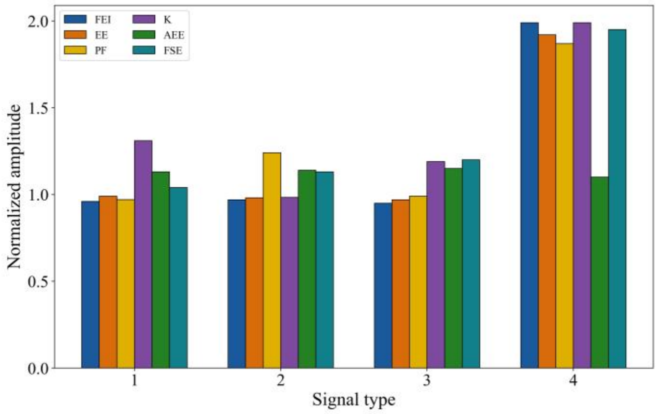

Figure 3. Comparison of various indicators for the four simulated signals.

3. Implementation of FMD adaptivity

This method significantly enhances the feature extraction precision of FMD through a parameter-adaptive optimization mechanism. Its core innovations lie in two aspects: First, a dynamic parameter search strategy based on swarm intelligence algorithms is established, overcoming the limitations of traditional empirical parameter settings. Second, a composite evaluation system is constructed by integrating physical characteristics such as impact periodicity indices, forming a multi-dimensional fitness function with fault-sensitive properties. The synergy between these two aspects enables FMD to rapidly converge to the optimal solution domain within the parameter space, thereby effectively improving the resolution of envelope spectrum features for typical faults like outer race cracks and roller spalling.

3.1. Theory of IVYA

Proposed by Mojtaba Hashemi et al. in 2024 [21], the IVYA is a novel metaheuristic approach based on the coordinated growth mechanisms of ivy colonies in nature. The IVYA algorithm demonstrates strong global optimization capability, avoiding convergence to local optima caused by individual search strategies. Furthermore, compared with particle swarm optimization (PSO), IVYA offers faster convergence speed, fewer parameters, and simpler computation procedures [21]. It also efficiently handles noise interference and volatility in fault data while ensuring fast convergence to stably approach local optima within shorter timeframes. Thus, this study employs IVYA to automatically locate the optimal key parameters for FMD. The algorithm mathematically formalizes the structured dispersion behaviour of ivy populations through a system of differential equations, with particular emphasis on proximity-based information exchange processes between individual plants. Each ivy agent autonomously determines its optimal growth direction within the solution space by dynamically analysing the fitness distribution of neighbouring individuals. This mechanism prioritizes tracking the trajectories of higher-fitness neighbours, thereby establishing a "local-following-global-exploration" co-evolutionary pattern. IVYA innovatively maps the spatial competition-cooperation dynamics observed in plant communities into a balanced exploitation-exploration strategy for optimization. Its distinctive growth dynamics model remarkably enhances the capability of the algorithm to avoid local optima. Based on the theory proposed by Mojtaba Hashemi et al. [21], the workflow of the algorithm is outlined as follows.

Step 1: Initialization:

Once the search space has been defined, the algorithm **proceeds to** the random initialization of the ivy population's positions. This step is crucial to ensure initial diversity across the search domain and is expressed mathematically as:

$$L_i = L_{min} + rand(1,E) \odot (L_{max} - L_{min}), i = 1, \dots, Npop \quad (5)$$

Where $rand(1,E)$ denotes an E-dimensional vector of uniformly distributed random numbers from the interval [0,1], L_{max} and L_{min} are the upper and lower bounds of the search space, "$\odot$" represents the Hadamard product between two vectors, and Npop indicates the population size.

Step 2: Coordinated and Structured Population Growth:

The growth rate Gp of each ivy plant is formulated as:

$$\frac{dGp(t)}{dt} = \psi \cdot Gp(t) \cdot \varphi(Gp(t)) \quad (5)$$

In this context, Variable Gp represents the growth rate, which quantifies the relative change over time. Variable ψ signifies the growth velocity (the absolute change rate), and Variable φ is the corresponding correction factor applied to address growth deviation. In the proposed algorithm, Eq.6 is rigorously derived through extensive experimental simulations and implemented via the following differential equation to model the growth velocity of the structural component L_i:

$$\Delta Gp_i(t+1) = rand^2 \odot (N(1,E) \odot \Delta Gp_i(t)) \quad (6)$$

Let $\Delta Gp_i(t)$ and $\Delta Gp_i(t+1)$ denote the growth rate of the discrete-time system at time steps t and t+1, respectively. The term $rand^2$ denotes a random number sampled from a random variable with a probability density function (PDF) equal to $1/(2\sqrt{x})$.

Step3: Sunlight Acquisition through Growth:

Ivy's epiphytic strategy exhibits remarkable ecological adaptability: its seedlings develop directional climbing behaviours driven by phototropism, preferentially attaching to microhabitats with mature support structures (e.g., tree trunks, rock surfaces). This intra-specific cooperation mechanism manifests as young vines spatially extending along established biological pathways formed by mature vines, creating continuous canopy coverage networks. Ecological studies reveal that this growth pattern triggers intense resource competition effects, where only individuals with optimal light-capturing efficiency and adhesion strength survive through natural selection. The dual mechanism of "path-dependent competition screening" ensures both rapid spatial expansion and ecological stability of the population, significantly influencing • L_i in the population, the movement toward light sources by selecting the strongest neighbouring individual L_{ii} is modelled as:

$$L_i^{new} = L_i + |N(1,E)| \odot (L_{ii} - L_i) + N(1,E) \odot \Delta Gp_i, \quad i = 1,2,\cdots,Npop \tag{7}$$

Where:

$$L_{ii} = \begin{cases} L_{j-1}^s, I_i = L_j^s \\ L_i, L_i = L_{Best} \end{cases} \tag{8}$$

$$\Delta Gp_i = \begin{cases} L_i \otimes (L_{max} - L_{min}), Iter = 1 \\ rand^2 \odot (N(1,E) \odot \Delta Gp_i), Iter > 1 \end{cases} \tag{9}$$

where $|N(1,E)|$ is a vector whose components are the absolute values of the components of vector $N(1,E)$, "$\oslash$" denotes the Hadamard division (element-wise division) between two vectors, and $Iter$ represents the iteration count.

Step 4: Propagation and Evolution of Ivy Population:

Upon completing the global exploration phase, each individual L_i first evaluates the population's fitness distribution to identify the current global best solution L_{Best}. It then establishes a gradient-tracking model centered on L_{Best}, constructing a dynamically contracting search radius within the neighbsdorhood of L_{Best} to perform high-precision solution space exploitation and update its growth rate. This mechanism is modeled by the equation:

$$\begin{cases} L_i^{new} = L_{Best} \odot (rand(1,E) + N(1,E) \odot \Delta Gp_i) \\ \Delta Gp_i^{new} = L_i^{new} \otimes (L_{max} - L_{min}) \end{cases} \tag{10}$$

Where ΔGp_i^{new} denotes the updated growth rate of the current member L_i^{new}.

3.2. Construction of a novel composite health indica-tor

The health indicator is a critical determinant of whether adaptive FMD can precisely and efficiently extract fault features from rolling bearings. This section discusses the construction of a high-performance composite health index (EPCHI) integrating EE and PF, which serves as the objective function for the optimization algorithm. Wei et al. [22] employed EE as the objective function in the whale optimization algorithm (WOA) to optimize key parameters of variational mode decomposition (VMD). It is considered an indicator of sparsity. Periodicity increases the sparsity of vibration signal and reduces EE accordingly.Based on the time-frequency localization property of the Hilbert transform, EE measures signal sparsity by quantifying the signal envelope's energy characteristics The mathematical mechanism is as follows:

$$H = -\sum_{t=1}^{N} \left(\frac{A(t)}{\sum_{t=1}^{N} A(t)} \right) ln \left(\frac{A(t)}{\sum_{t=1}^{N} A(t)} \right) \tag{11}$$

$$A(t) = |\text{Hilbert}(IMF_k(t))| \tag{12}$$

Where $A(t)$ is the envelope amplitude of the *k-th* intrinsic mode function (IMF) component after Hilbert transform, and $A(t)/\sum_{i=1}^{N} A(t)$ represents the normalized envelope amplitude. However, the EE as a sparsity characterization metric suffers from three theoretical limitations. First, its mathematical essence is a complexity measure based on Shannon entropy theory for envelope energy distribution, which differs in physical interpretation from classical sparsity metrics such as the kurtosis factor. This leads to feature misidentification when processing non-impulsive sparse signals like broadband modulated faults. Second, the Hilbert demodulation process is susceptible to endpoint effects caused by Gibbs phenomena, particularly in non-stationary signal processing, where amplitude distortion at boundary regions results in falsified energy distribution in envelope spectra. Third, the EE metric calculates entropy solely from normalized envelope energy, disregarding transient impact intensity information encoded in the absolute amplitude of raw signals. The PF characterizes the strength of vibrational pulses in signals and is effective in detecting impulsivity [23]. The impulsiveness of signals exhibits a positive correlation with the PF value, and the PF value increases as the signal impulsiveness grows. The pulse factor I is computed as:

$$I = \frac{A_{pk}}{\frac{1}{N}\sum_{t=1}^{N} A(t)} \tag{13}$$

Where I and A_{pk} are the impulse factor and peak-to-peak value of the vibration signal, respectively. The PF exhibits high sensitivity to impulsive characteristics in vibration signals and computational efficiency, but it also has the following limitations: First, its fourth-order statistical moment properties render it highly sensitive to non-fault transient disturbances, such as mechanical impacts and electromagnetic pulse interference. Second, it demonstrates low robustness against noise.

To better characterize the sparsity and impulsiveness of signals, a novel composite health index (CHI), termed EPCHI, is designed. Since both EE and PF are dimensionless values, EPCHI is constructed using the following equation:

$$EPCHI = \frac{H}{I} \tag{14}$$

As derived in Eq.(15), EPCHI serves as a dual indicator of signal sparsity and impulsiveness, exhibiting a negative correlation with both parameters: specifically, EPCHI decreases as either characteristic intensifies.

4. The proposed fault diagnosis model

4.1. Model Construction

The proposed fault diagnosis model addresses the issue where traditional FMD parameters are empirically preset, often leading to over-decomposition and mode aliasing. This method integrates FMD with adaptive parameter selection with a novel composite health indicator (CHI). In this framework, the IVYA serves as the optimization algorithm, and the EPCHI is utilized to construct the optimization's fitness function. The parameter optimization of FMD is formulated as a problem of minimizing the EPCHI value. Eq. 16 provides the mathematical expression for the fitness function. Where L, n, and $p_i = (n.L)$ represent the filter length and mode number of the FMD and the position of the *i-th* Ivy agent, respectively.

$$fitness = min_{p_i=(n,L)}(EPCHI_{p_i}) \tag{15}$$

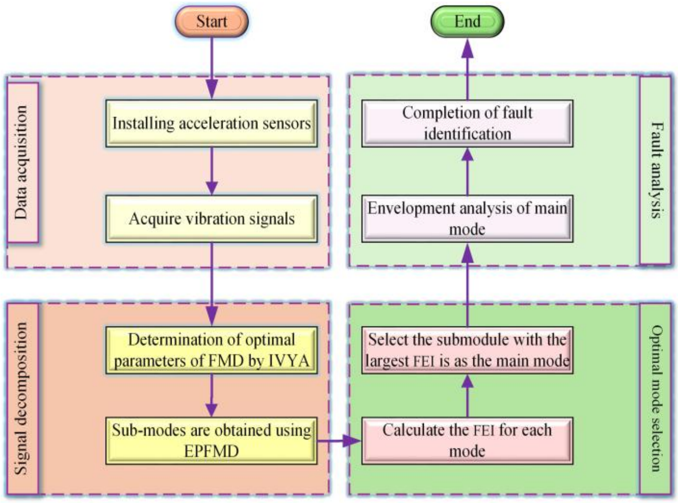

Figure 4. Flowchart of the proposed adaptive FMD.

Fig. 4 illustrates the workflow of the proposed model, with detailed steps outlined below:

(1) The vibration signals acquired by the accelerometer are input into the model. The IVYA is then initialized with a maximum iteration count of 20 and a population size of 20. The lower bound $lb = [n_{min}, L_{min}]$ and upper bound $ub = [n_{max}, L_{max}]$ for the key parameters of FMD are determined by balancing computational efficiency and decomposition accuracy. For the mode count n, a value too small causes mode aliasing (insufficient feature extraction for bearing defects), while a value too large leads to excessive computational load and over-decomposition. It has been empirically demonstrated that setting the parameter n to a value between 2 and 7 optimally balances the requirement for high feature resolution against the constraints of computational cost. For the filter length $L_{max} \leq round(f_s/f_g)$, the maximum is constrained by a dual-ratio mechanism based on the sampling frequency f_s and bearing fault frequency f_s, ensuring a balance between computational complexity and time-frequency resolution. This strategy avoids excessive filtering (reducing computational waste) while retaining critical fault signatures. Frequency ratio analysis preserves fault-related spectral components, enabling effective feature extraction. The upper and lower bounds of the FMD parameters are defined as given in Eq.17, where the function round denotes the rounding operation [24].

$$\begin{cases} ub = \left[7, \leq round(\frac{f_s}{f_g})\right] \\ lb = [2,2] \end{cases} \tag{16}$$

(2) Pattern decomposition of input signals using preset

parameters.

(3) Within the predefined iteration count, the fitness function of each mode is iteratively computed.

(4) The optimal parameter combination is selected through fitness function comparison, with the corresponding mode count n and filter length L recorded.

(5) FEI values of all sub-modes are calculated and evaluated, based on the criterion of maximizing the FEI, the corresponding mode is selected as the dominant component, as it contains the most significant fault-related information

(6) Envelope spectrum analysis is performed on the identified principal mode to achieve precise identification of fault characteristic frequencies.

Table 1. Specific parameters of h(t).

M_1	M_2	M_3	f_1	f_2	f_3	θ_1	θ_2	θ_3
0.2	0.2	0.4	63	160	6.5	π/6	-π/3	0

4.2. Validation of the method with simulated signals

4.2.1. Modeling of bearing faults using simulation

A benchmark modulated signal is synthesized based on the known physical characteristics of bearing defects. This synthetic signal serves as a ground-truth test case for benchmarking the performance of the EPFMD algorithm, as detailed below.The simulated signal consists of random impulses $r(t)$ induced by sudden impacts, background noise $n(t)$ with standard deviation σ=0.900, periodic impulses $p(t)$ caused by bearing faults, and harmonic components $h(t)$ from rotational frequency, [25].

$$\begin{cases} p(t) = \sum_i P_i \cdot e^{-\alpha_1 (t-i) f_o - \Delta/f_o} \, sin(\, 2\pi f_{n1} (t - i/f_o - \Delta/f_o) \\ r(t) = \sum_j^J D_j \cdot e^{-\alpha_2 (t-\varepsilon_j)} \, sin(\, 2\pi f_{n2} (t - \varepsilon_j) \,) \\ h(t) = M_1 \, sin(\, 2\pi f_1 t + \theta_1) + M_2 \, sin(\, 2\pi f_2 t + \theta_2) \\ \qquad + M_3 (0.5 + 0.3 \, sin(\, 2\pi f_3 t + \theta_3)) \\ n(t) = \sigma \cdot \mathcal{N}(0,1) \\ x(t) = p(t) + r(t) + h(t) + n(t) \end{cases} \tag{17}$$

In $p(t)$, the magnitude P_i of the i-th periodic impulse follows a uniform distribution $U \in [0.9,1]$. The bearing fault characteristic frequency f_o is 100Hz. The resonant frequency f_{n1} and decay coefficient α_1 are 2340 Hz and 860 rad/s, respectively. Speed fluctuations are simulated by the time jitter Δ generated from a uniform distribution $U \in [-0.02, 0.02]$.

The two key parameters of r(t) are defined as follows: the number of random shocks is denoted by J, and the intensity of these shocks is represented by D_j, with the value for both parameters being 2. The parameters for the j-th random shock are set as follows: occurrence time ϵ_j=2, decay frequency f_{n2}=4300 Hz, and damping coefficient α_2=600 rad/s.

In the signal model $h(t)$, the i-th harmonic component is parameterized by its amplitude (P_i), frequency (f_i), and phase (θ_i). The specific values for these parameters are provided in Table 1. Data collection was performed at a sampling frequency of 16,000 Hz with 10,000 samples. As illustrated in Fig. 5, despite the capability of direct spectral analysis (using both the amplitude spectrum and squared envelope spectrum) to identify certain harmonic interference components (f_1, f_2), it does not reveal the characteristic frequency (f_o) associated with the bearing fault. This shortcoming underscores a fundamental limitation: the periodic impulse fault signature within $x(t)$ is effectively masked by noise and cannot be recovered through conventional spectral techniques alone. This finding highlights the necessity for more advanced signal processing methods to achieve effective fault diagnosis.

4.2.2. Validation of the proposed method

Analysis of the aforementioned simulated signal was carried out using the proposed method. First, a optimization algorithm with EPCHI was employed to select the optimal combination parameters (i.e., filter length L and mode number n) as 57 and 4, respectively. Employing the parameter-optimized FMD, the simulated signal was decomposed, yielding four distinct mode components. Fig. 6 presents the decomposition results. Fig. 7(a) presents the FEI values calculated for the four mode components derived from the decomposition. The results indicate that the fourth component attains the maximum FEI value. Consequently, it is identified as the most fault-sensitive component and selected for subsequent envelope spectrum analysis to detect the characteristic frequency associated with the fault. The envelope spectrum of the dominant mode is presented in Fig. 7(b). it clearly reveals the characteristic frequency (f_o = 100 Hz) associated with the bearing fault along with its harmonics up to the sixth order ($2f_o$, $3f_o$, ..., $6f_o$). This result successfully validates the effectiveness of the proposed approach in identifying bearing defect characteristics.

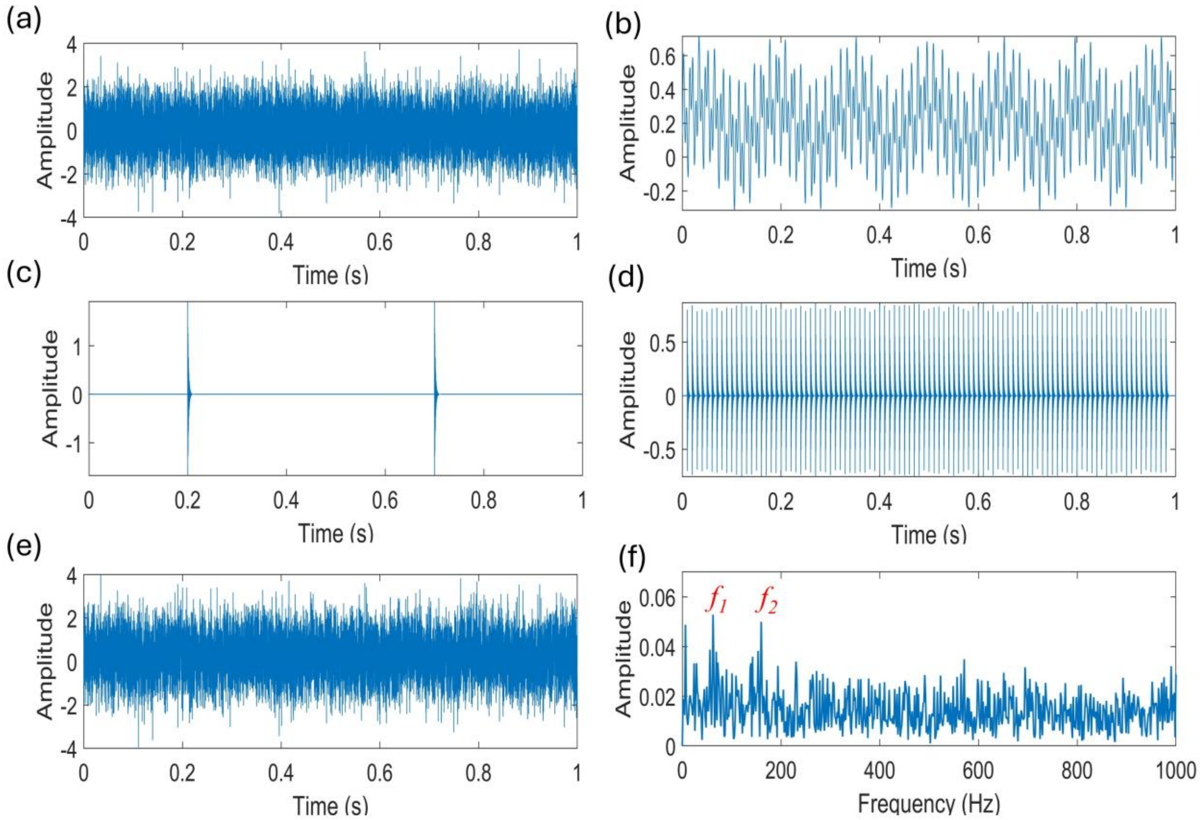

Figure 5. Simulated signal: (a) Gaussian white noise n(t); (b) discrete harmonic interference signal h(t); (c) random impact r(t); (d) Cycle impact p(t); (e) bearing fault simulation signal x(t); (f) simulated signal's envelope spectrum.

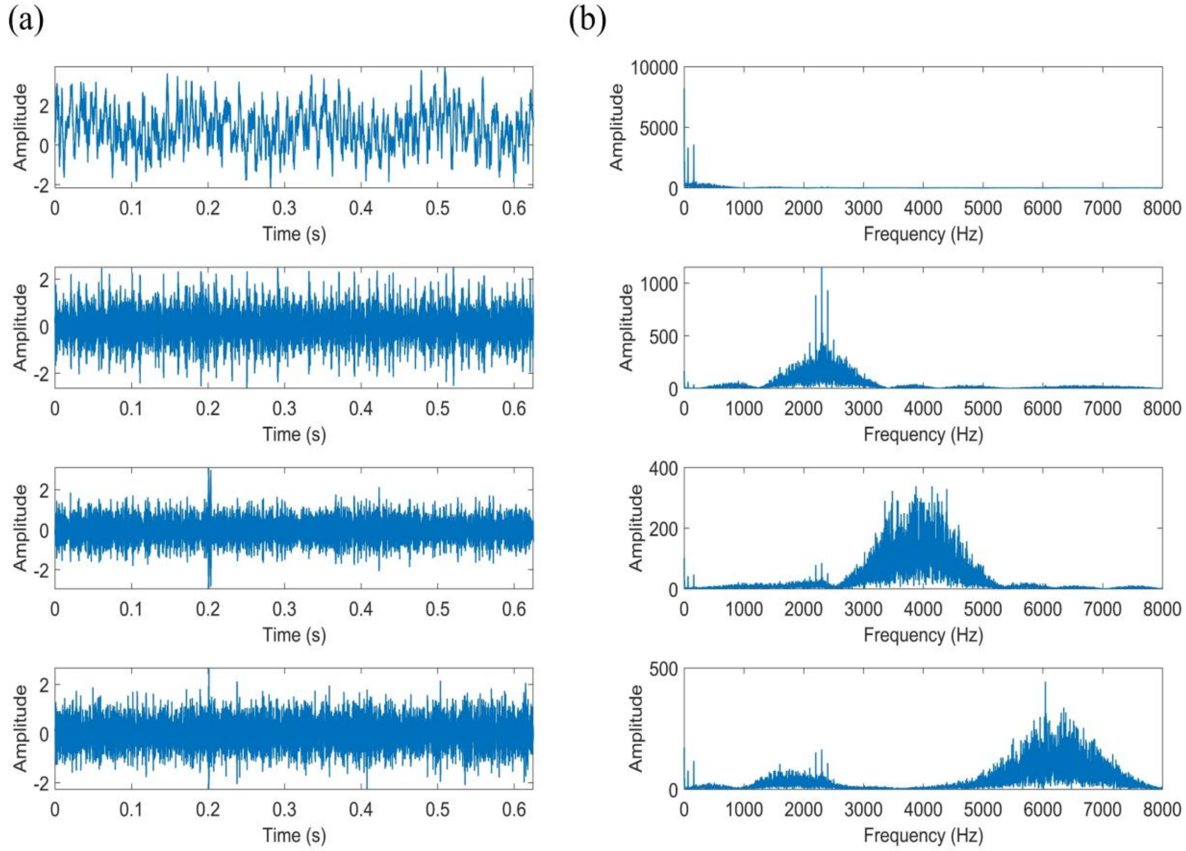

Figure 6. (a) Mode Components and (b) the corresponding envelope spectrum derived from the simulated signal using EPFMD.

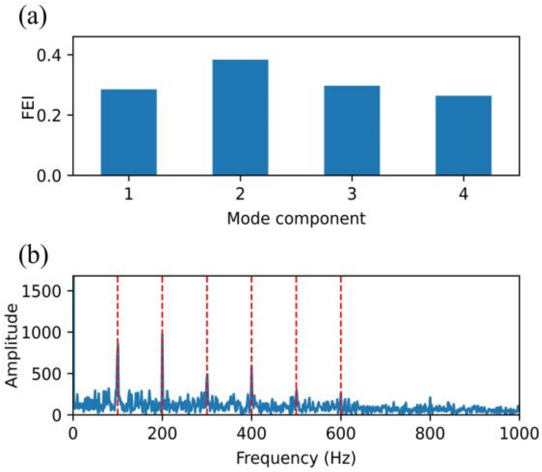

Figure 7. Analysis results of the simulated signal processed by the EPFMD method: (a) FEI values for all decomposed modes, (b) envelope spectrum of main mode.

5. Validation and analysis through experiments

5.1. Dataset validation

Section 5.1 describes validation conducted with the Case Western Reserve University (CWRU) bearing dataset [26], a widely used benchmark in bearing fault diagnosis. The CWRU test rig consists of a 2-hp motor, a torque transducer/encoder, and a load dynamometer. For experimental validation, test bearings with prefabricated localized defects generated by electrical discharge machining (EDM) were installed at two critical transmission nodes: at the drive-end coupling and the non-drive end (fan side) bearing housing. A dual-channel data acquisition system was employed, operating with base and high-frequency sampling rates of 12 kHz and 48 kHz, respectively, and a sampling duration of 10 seconds per channel. The analysis utilized drive-end inner race fault data characterized by a depth of 0.011 inches (0.2794 mm) and fault diameter of 0.07 inches (0.1778 mm). The tests were conducted under operational conditions of a 0.735 kW load and a rotational speed of 1772 r/min. The specifications of the bearing model used are detailed in Table 2 [25].

Table 2. Parameters of CWRU bearing.

Parameter category	Parameter
Bearing model	SKF-6205-2RS
Position on the motor	Drive end
Pitch diameter	39.04mm
Roller diameter	7.94mm
Number of balls	9
Contact angle	0°

5.1.1. Noise is injected into the fault signal

To examine the robustness of the proposed method in diagnosing faults under noise interference, the experiment utilized low-noise raw signals acquired in an ideal testing environment as baseline data. Noise-contaminated samples were constructed by injecting -5 dB Gaussian white noise into the original signals. Fig. 8 illustrates the time-domain waveforms and envelope spectrum of both the original and noise-contaminated signals.

As can be seen in Fig. 8, the original signal exhibits clear periodic impulsive features in both the time-domain waveform and envelope spectrum. In contrast, the noise-contaminated signal displays significant distortion in the time-domain waveform, appearing chaotic with no observable impulsive characteristics, while its frequency spectrum shows a marked increase in high-frequency interference components. Notably, the envelope spectrum of the original signal reveals a prominent peak at the fault characteristic frequency f_g, and its harmonics ($2f_g$, $5f_g$), whereas this peak is severely attenuated in the noise-contaminated case, with most features entirely submerged by background noise. This validates the typical failure of conventional diagnostic methods under high-noise conditions.

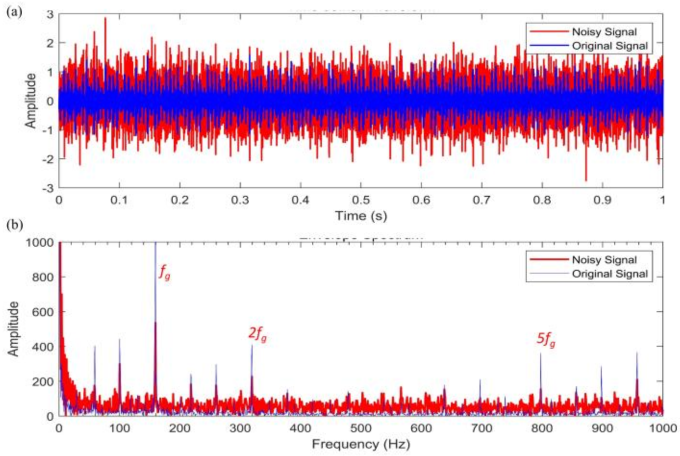

Figure 8. (a) Time domain waveform and (b) envelope spectrum of noisy signal.

To demonstrate the necessity of FMD parameter optimization, Feature mode decomposition was performed on the noise-contaminated signal using randomly preset parameters (L=60, n=4), yielding four IMFs. As illustrated in Fig. 9, the fault characteristic frequency (f_g) and its second harmonic ($2f_g$) are only faintly discernible in the envelope spectrum of IMF2 (Fig. 9(a)), exhibiting negligible amplitude and poor prominence. Crucially, no fault-related features are identifiable in the remaining IMF components. This result underscores the critical importance of optimizing FMD parameters to achieve effective feature separation.

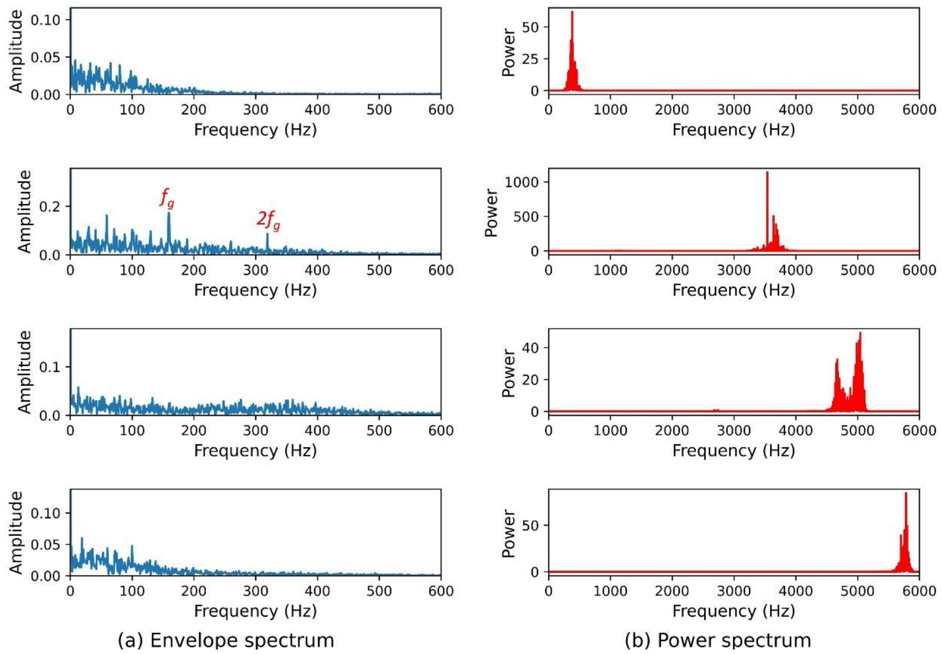

Figure 9. The (a) envelope spectrum and (b) power spectrum of each decomposed component after FMD.

5.1.2. Application of the proposed methodology

Next, the EPFMD method was used to conduct parameter-adaptive decomposition on the noise-contaminated signal. To balance computational efficiency against decomposition accuracy, the maximum allowed number of iterations was 20. The parameters to be optimized—mode number *n* and filter length *L*—were bounded within the ranges of [2, 7] and [2, 60], respectively. Applying this FMD with adaptive parameter selection to the signal yielded a decomposition into seven IMF components (Fig. 10). With the aim of obtaining a trade-off between computational efficiency and decomposition accuracy, the optimization process was configured with an iteration limit of 20. The search space for the parameters *n* and *L* was defined by the predefined bounds (*ub* = [7, 60], *lb* = [2, 2]). Consequently, the application of FMD with these settings resulted in a signal decomposition into seven IMFs, detailed in Fig. 10.

The FEI was calculated for each mode, with results shown in Fig. 11(a). IMF4 was identified as the optimal mode for envelope analysis due to its highest FEI value. The corresponding envelope spectrum (Fig. 11(b)) distinctly reveals the inner race fault characteristic frequency (f_g = 159.9 Hz) and its harmonics ($2f_g$ to $6f_g$), all marked in red, with high amplitude saliency. This clear identification of fault-related frequencies under significant background noise demonstrates the method's high efficacy in diagnosing bearing inner race defects.

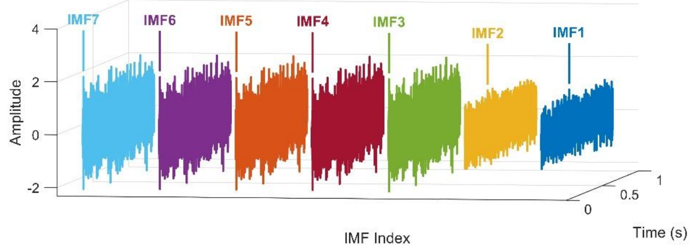

Figure 10. EPFMD decomposition outcomes for the CWRU dataset.

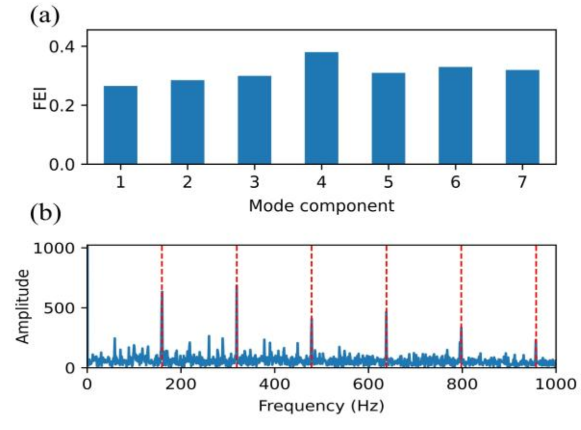

Figure 11. The processing results of the CWRU dataset using the EPFMD method. (a) FEI values of the each mode. (b) envelope spectrum of the dominant mode component.

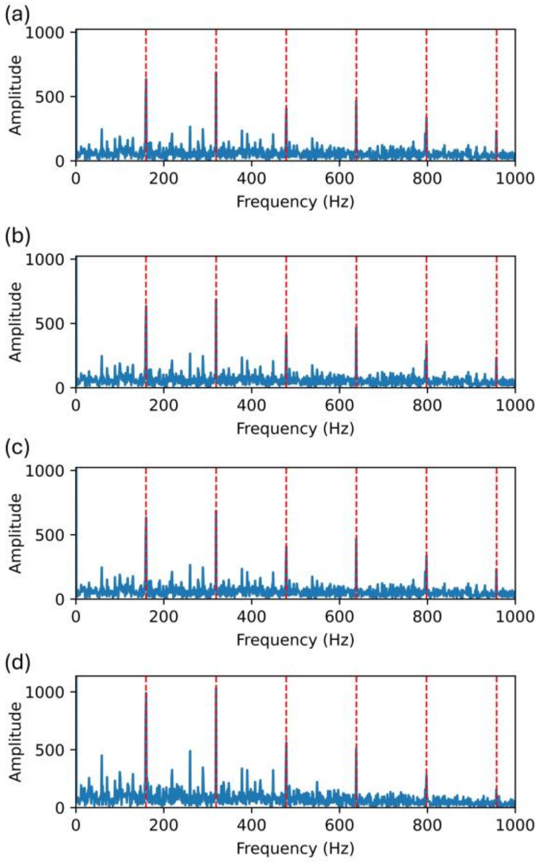

Figure 12. EPCHI is used as fitness function, and different optimization algorithms are used to optimize FMD: (a) COA, (b) SSA, (c) DBO, (d) ZOA.

A series of experiments for comparison was performed to validate the superiority of the EPFMD method in rolling bearing fault diagnosis. With the EPCHI serving as the fitness function to guide the optimization process, four optimization algorithms-Crayfish Optimization Algorithm (COA), Sparrow Search Algorithm (SSA), Zebra Optimization Algorithm (ZOA), and Dung Beetle Optimizer (DBO)-were independently applied for FMD with adaptive parameter selection decomposition. The FEI was computed for each resulting IMF). The mode with the highest FEI value was subsequently identified and subjected to envelope spectrum analysis, with the corresponding results displayed in Fig. 12. As shown in the figure, the use of COA, SSA, and DBO as optimization algorithms achieved diagnostic effects comparable to IVYA, with identical amplitude saliency. However, when ZOA was used as the optimization algorithm, the amplitude saliency of the $6f_g$ harmonic was significantly weaker. Fig.13 presents the iteration curves of all optimization algorithms evaluated in this study. It can be observed that SSA and IVYA exhibit the fastest convergence speeds, outperforming other algorithms.

This demonstrates the significant superiority of IVYA as an optimization algorithm for FMD in diagnosing bearing inner race faults.

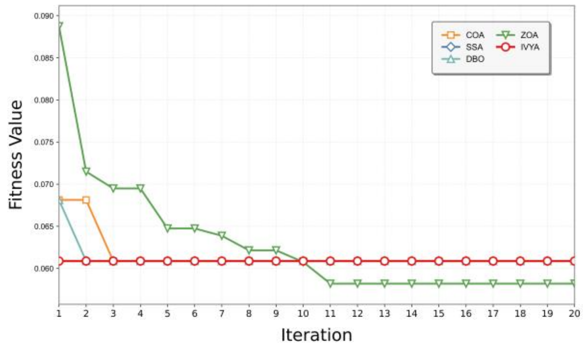

Figure 13. A comparison of the convergence characteristics of different optimization algorithms.

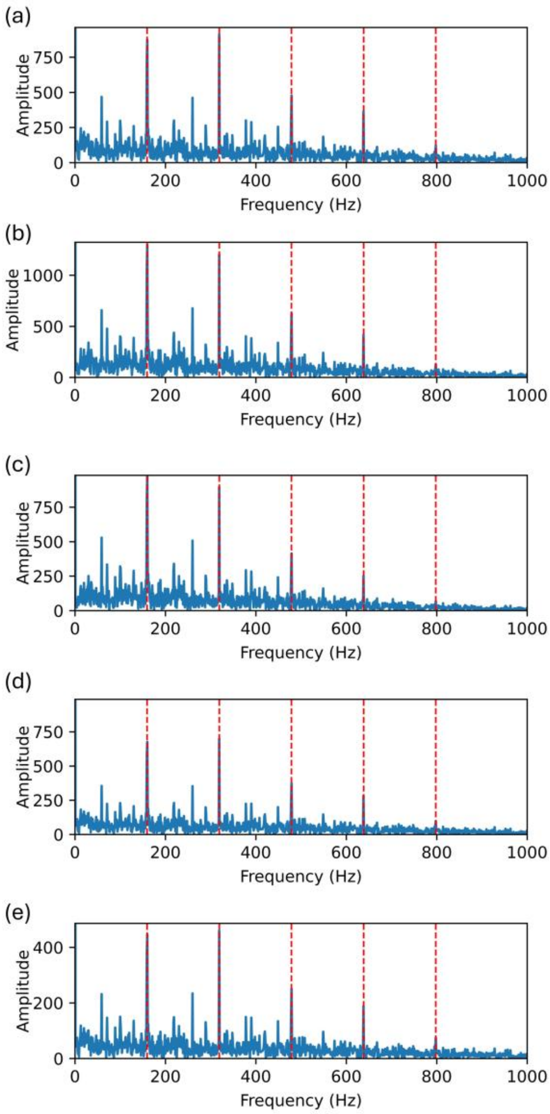

Figure 14. IVYA is used as optimization algorithm, and different fitness functions are used to optimize FMD: (a) EE, (b) PF, (c) K, (d) AEE, (e) ESPF.

Next, using IVYA as the optimization algorithm, different fitness functions—EE, PF, kurtosis, average envelope entropy (AEE), and envelope spectrum peak factor (ESPF)—were tested for FMD with adaptive parameter selection. The FEI values was computed for each resulting IMF. The component exhibiting the highest FEI value was consequently identified as the principal mode and subjected to envelope spectrum analysis. Fig. 14 showing the results of this analysis. Observations reveal that these methods could only extract the inner race defect characteristic frequency fg and its 2nd to 5th harmonics (2fg to 5fg), with poor noise suppression resulting in weak amplitude saliency. This validates the superiority of EPCHI as the fitness function for identifying bearing inner race defects.

The comparative analyses presented above constitute a longitudinal study design. The superiority of the EPFMD method is further verified through a series of horizontal comparative decomposition (IVYA-SVMD), IVYA-optimized variational mode decomposition (IVYA-VMD), empirical wavelet transforms (EWT), and simplistic geometric mode decomposition (SGMD). A comparison of the fault feature extraction capabilities is illustrated in Fig. 15. Specifically, subfigure (a) (IVYA-SVMD), (b) (IVYA-VMD) and subfigure (c) (EWT) both successfully identify the fundamental fault characteristic frequency (f_g) and its subsequent three harmonics ($2f_g$ to $4f_g$) but failed to identify $5f_g$ and $6f_g$, with weak amplitude saliency due to noise interference. Fig. 15(d) reveal that only f_g and $2f_g$ were extracted when SGMD were applied, with significantly fewer harmonics and lower amplitudes compared to the proposed method. These results confirm the inferior diagnostic performance of these methods for inner race faults relative to EPFMD.

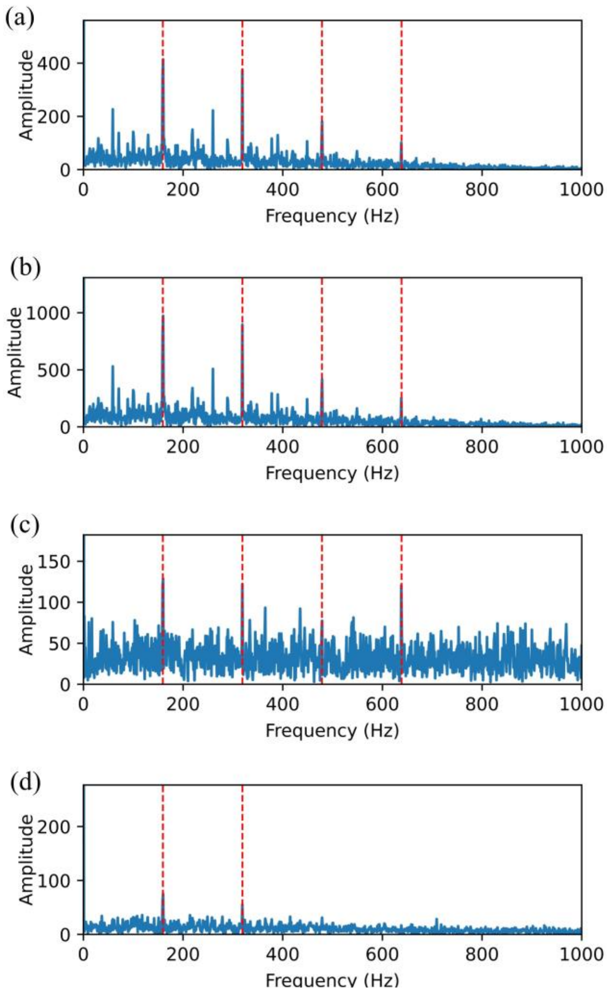

Figure 15. Results of four different methods:(a) IVYA-SVMD, (b) IVYA-VMD, (c) EWT, (d) SGMD.

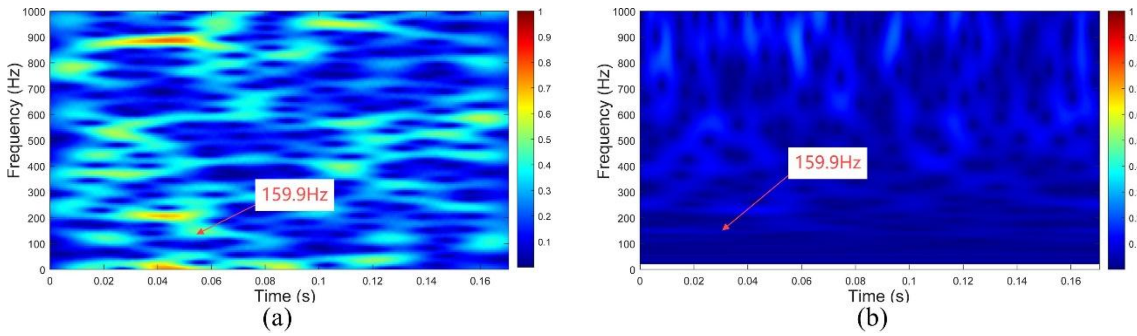

Figure 16. Processing results of two different time-frequency processing methods: (a) STFT, (b) GST.

Fig. 16(a) and (b) illustrate the results of two common time-frequency analysis methods—short-time Fourier transform (STFT) and generalized S-transform (GST)—applied to the fault signal. While STFT (Fig.16(a)) identifies f_g, severe background noise obscures its saliency, and no harmonics are detected. Similarly, SST (Fig. 16(b)) weakly captures f_g but fails to resolve harmonics under strong noise. Finally, a comparative analysis was conducted with advanced improved FMD methods: Parameter-Optimized Feature Mode Decomposition (POFMD) [24] and Adaptive Health Index-based FMD (AHA-FMD) [13]. It should be noted that the modal with the largest FEI in the decomposition results was similarly selected as the optimal component for subsequent analysis in the POFMD as well as AHA-FMD approaches. The processing outcomes are displayed in Figs. 17(a) and (b), respectively. From Fig. 17(a), the POFMD approach effectively extracts the characteristic frequency f_g of the rolling bearing fault. However, the spectral analysis reveals the presence of only a single harmonic, identified as the second-order component ($2f_g$), and its spectral peaks demonstrate poor amplitude significance due to noise contamination. The diagnostic results of the AHA-FMD method in Fig. 17(b) reveal that both the fault frequency f_g and the four harmonics ($2f_g$ to $5f_g$) are extracted. Nevertheless, amplitude significance as well as harmonic component count remain inferior to the proposed EPFMD approach.

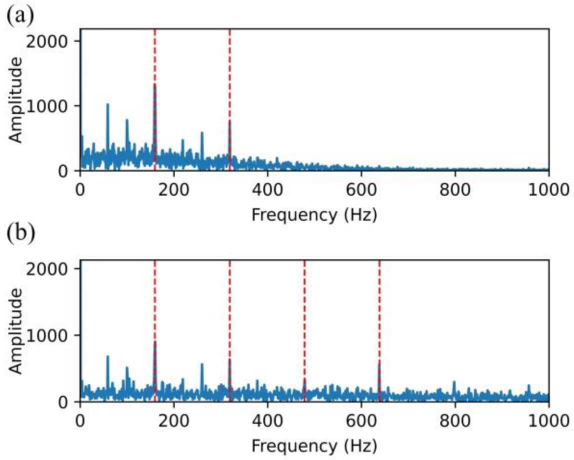

Figure 17. Results of two different methods: (a) POMD, (b) AHA-FMD.

In summary, through vertical, horizontal, and comparative analyses with a series of improved FMD methods, EPFMD demonstrates distinct advantages in diagnosing inner-race faults of rolling bearings.

5.2. Experimental rig validation

To validate the bearing fault diagnosis performance of the proposed method in engineering scenarios, experimental validation was conducted using a PT870 bearing test rig (structural diagram shown in Fig. 18). The test object was a rolling bearing with prefabricated defects (fault morphology shown in Fig.19; specifications detailed in Table 3). A VAST-DC27 multichannel data acquisition system equipped with 16 accelerometers (see Table 4 for collector parameters and Table 5 for sensor specifications) established a three-dimensional vibration moni-toring network. This sensor array ensured spatiotemporal continuity in vibration signal acquisition and enabled multi-dimensional capture of fault-induced impulsive features.

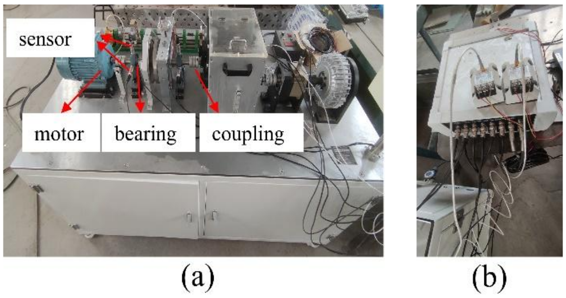

Figure 18. Fault diagnosis experimental rig.

Figure 19. Two kinds of fault bearings: (a) Outer race fault bearing, (b) Comprehensive fault bearing.

Table 3. Experimental stand bearing parameters.

Bearing model	Width	Outer Diameter	Inner Diameterr
CPH206	38mm	62mm	62mm

Table 4. Collector parameters.

Parameter category	Parameter
Instrument Model	VAST-DC27
Number of Measurement Channels	Sixteen channels
ADC Resolution	16-bit
Supported Sensor Types	Vibration, tachometer, eddy current dis-placement
Communication Interface	Ethernet
Operating Voltage	24V
Maximum Sampling Rate	Simultaneous sampling at 100 kHz
Power Supply	220 V AC adapter
Nonlinearity	±0.1%
Frequency Response	0.5 Hz–20 kHz

Table 5. Accelerometer parameters.

Parameter category	Parameter
Accelerometer mass	75g
Working temperature	-20-75℃
Frequency response	(+/-10%):0.6-10000HZ (+/-3dB):0.4-13000HZ
The protection grades	IP67
Transient response shock	50g peak(max 5000g)
Sensitivity	100mV/g +/- 10%

5.2.1. Case 1

In order to verify the efficacy of the proposed method for outer-race bearing faults, the vibration signal obtained was analyzed. Fig. 20 display the corresponding time-domain waveform and the results of the envelope spectrum analysis. Notably, the outer race fault characteristic frequency (f_o) exhibits no significant spectral peaks in conventional envelope spectra (bearing parameters detailed in Table 6), likely due to strong background noise or weak fault-induced impulsive energy. To overcome these limitations, the EPFMD method is used to process fault signals.

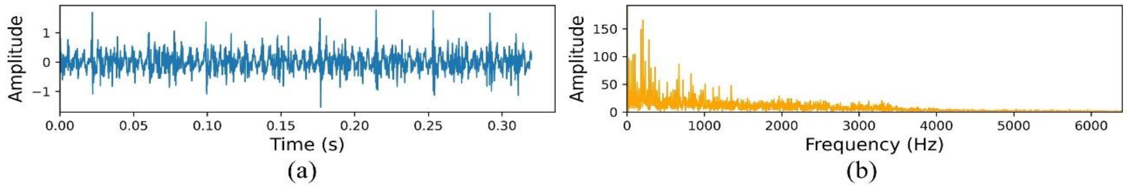

Figure 20. The (a) Time domain waveform and (b) Envelope spectrum of outer race fault bearing.

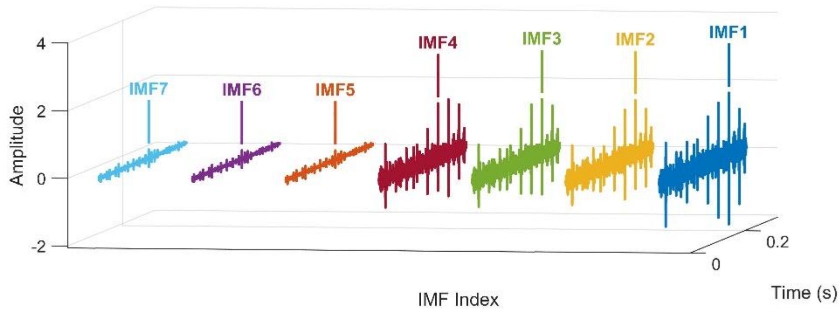

Figure 21. The processing result of EPFMD method to outer race fault signal.

Fig. 21 shows the processing results. The FEI values of all components were calculated (Fig. 22(a)). Using EPCHI and IVYA-optimized FMD parameters (n=7, L=40). For the subsequent envelope analysis, IMF6 was identified as the principal mode due to its highest FEI value. In the resulting envelope spectrum for case 1, the outer race fault characteristic frequencies and their harmonics are clearly highlighted in red.

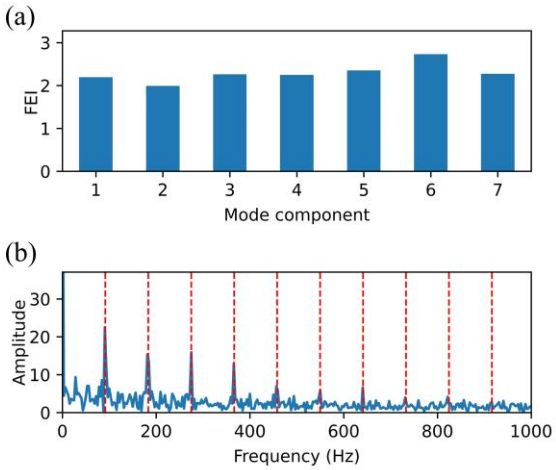

Figure 22. EPFMD-based processing results of the outer-race fault signal: (a) FEI values of the each mode. (b) envelope spectrum of the dominant mode component.

As shown in Fig. 22(b), the envelope spectrum of IMF6 clearly extracts the fundamental outer race fault frequency fo and its higher-order harmonics (2fo to 10fo). with high amplitude saliency. This demonstrates that EPFMD effectively diagnoses rolling bearing outer race fault even under challenging noise conditions.

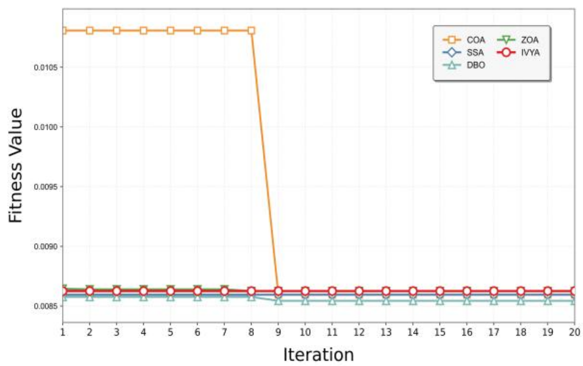

Figure 23. A comparison of the convergence characteristics of different optimization algorithms.

We evaluated the advantage of the EPFMD method through comparison of its performance against different approaches on the same signal. First, with EPCHI as the fitness function, four different distinct intelligent optimization algorithms (i.e., COA, SSA, DBO and ZOA) were employed for FMD with adaptive parameter selection. Fig. 23 shows the iteration curves of these algorithms. where IVYA demonstrates superior convergence speed. Each decomposition's mode with the highest FEI value was determined to be the principal mode for envelope analysis (results in Fig. 24). All methods successfully extracted the outer race fault characteristic frequency f_o and its harmonics ($2f_o$ to $10f_o$), confirming that EPCHI as the fitness function enables effective diagnosis of outer race defects across different optimization algorithms. Next, using IVYA as the optimizer, five alternative fitness functions (i.e. EE, PF, K, AEE and ESPF) were tested for FMD.

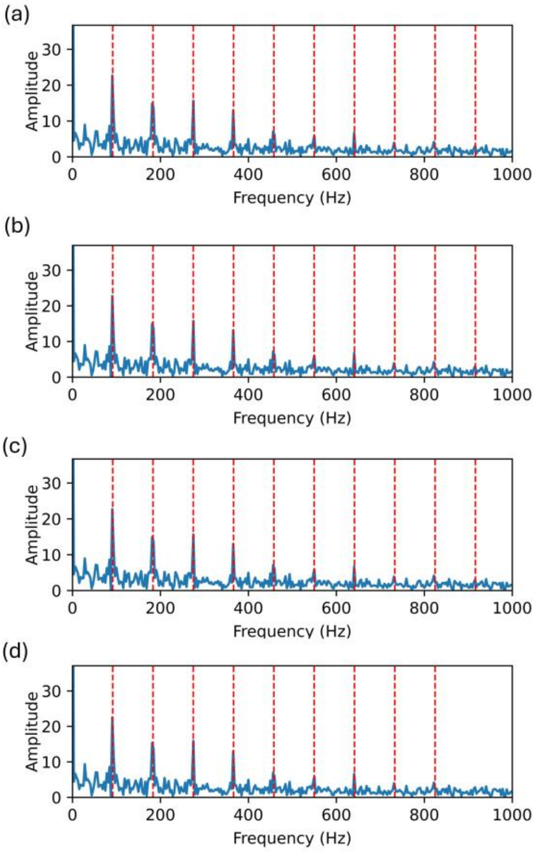

Figure 24. EPCHI is used as fitness function, and different optimization algorithms are used to optimize FMD: (a) COA, (b) SSA, (c) DBO, (d) ZOA.

The envelope spectra of the modes with the highest FEI values (Fig. 25) reveal that only the second harmonic (2fo) was detected, while the fundamental frequency fo remained obscured. This stark contrast underscores the significant superiority of the EPFMD method in longitudinal comparative experiments. In order to validate the effectiveness of the proposed method, a series of horizontal comparative experiments was conducted. Four methods referenced in Section 5.1 (i.e., IVYA-SVMD, IVYA-VMD, EWT and SGMD) were applied to process the outer race fault signal. The sub-mode characterized by the maximum FEI value was identified as the optimal component for sub-sequent envelope analysis. The outcomes of this analysis are presented in Fig. 26. For IVYA-SVMD, Fig. 26(a) shows the outer race fault frequency fo and its harmonics (2fo–4fo) were extracted, but fewer harmonics and weaker amplitude saliency were observed compared to EPFMD. The IVYA-VMD, EWT, and SGMD methods (Figs. 26(b), (c) and (d)) all extracted only the second harmonic (2fo) of the outer race fault and failed to successfully capture its fundamental frequency, with strong clutter interference present in the results. Although the amplitude of 2fo in EWT is relatively high, clutter spikes reduce its prominence. In SGMD, 2fo exhibits low amplitude, further confirming its poor diagnostic capability.

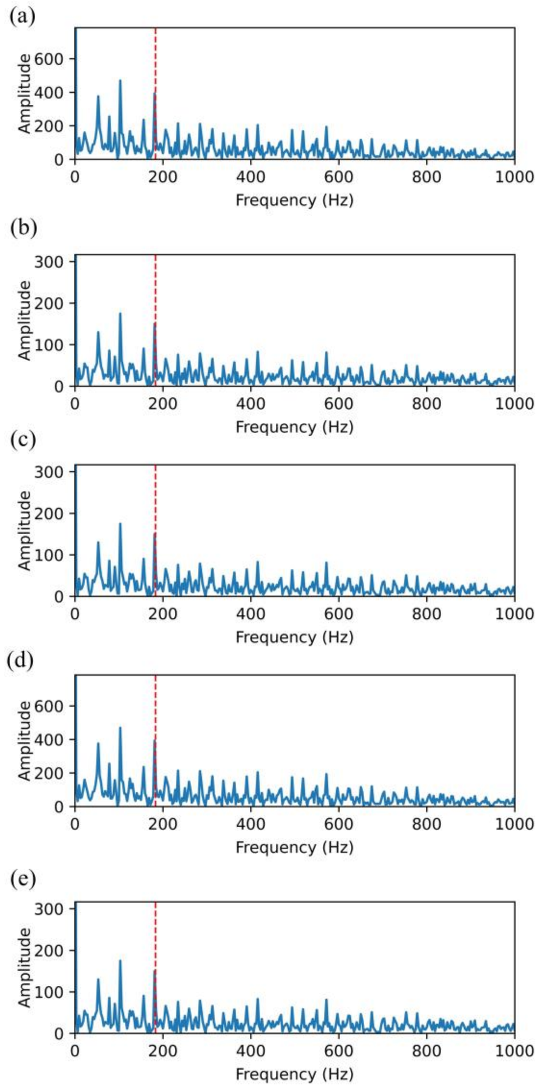

Figure 25. IVYA is used as optimization algorithm, and different fitness functions are used to optimize FMD: (a) EE, (b) PF, (c) K, (d) AEE, (e) ESPF.

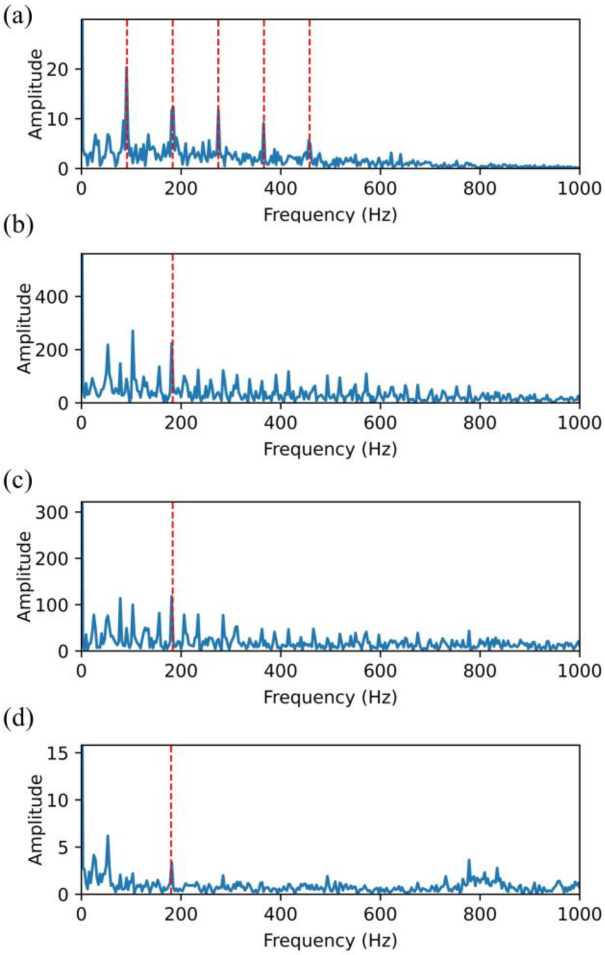

Figure 26. Results of four different methods: (a) IVYA-SVMD, (b) IVYA-VMD, (c) EWT, (d) SGMD.

We also processed the outer race bearing fault using two other time-frequency methods—namely, the Short-Time Fourier Transform (STFT) and the Generalized S-Transform (GST). The results are presented in Fig. 27. In the STFT meth-od, we can observed the harmonic components of the outer race fault characteristic frequency (2fo, 4fo, 5fo, and 6fo). However, the fundamental frequency fo remains unde-tected, with substantial background noise and multiple inter-ference components, resulting in poor diagnostic effective-ness.

The results of the GST method presented in Fig. 27(b) indi-cate that the harmonics of the outer-race fault (2fo and 4fo) are apparent, but the fundamental frequency fo is missing. Additionally, background noise interference is more pro-nounced, resulting in poor saliency of defect features.

Likewise, to provide further evidence of the proposed method's performance, its fault diagnosis was benchmarked against two advanced FMD variants: POFMD and AHA-FMD. The POFMD and AHA-FMD methods were respective-ly applied to process rolling bearing outer race fault signals, with the mode with the maximum FEI value was conse-quently identified as the dominant mode and subjected to envelope spectrum analysis. Figs. 28(a) and (b) shows the results. Fig. 28(a) clearly reveals the characteristic frequency (fo) corresponding to the outer race fault. Additionally, six fault harmonics (2fo to 7fo) are identified; however, the har-monic count remains inferior to that achieved by the EP-FMD method. The analysis results obtained by the AHA-FMD method, as presented in Fig. 28(b), successfully identify the fundamental fault characteristic frequency (fo) along with its first three harmonics (2fo to 4fo). Similarly, the quantity of extracted harmonics is limited.

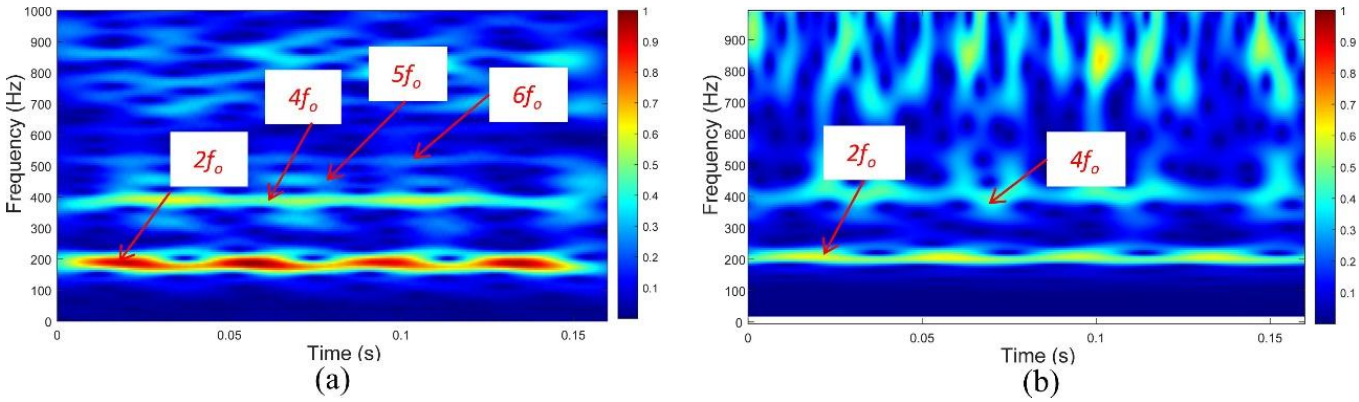

Figure 27. Processing results of two different time-frequency processing methods: (a) STFT, (b) GST.

In summary, based on the above experiments, the proposed method demonstrates significant superiority in diagnosing rolling bearing outer race faults.

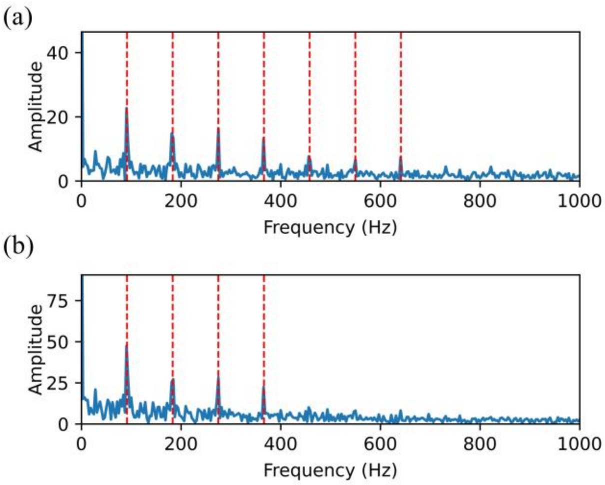

Figure 28. Results of two different methods: (a) POMD, (b) AHA-FMD.

5.2.2. Case 2

Prior research have validated the excellent diagnostic per-formance of the EPFMD method in identifying rolling bear-ing faults involving both inner and outer races demonstrating its marked superiority over conventional diagnostic ap-proaches. However, all tested faults occurred individually. In practical applications, bearing faults often manifest as com-prehensive faults involving multiple concurrent defects. To demonstrate the applicability of the proposed method to comprehensive bearing fault diagnosis, the outer race fault bearing was replaced with a comprehensive fault bearing containing outer race, inner race, and rolling-element defects. Details of the comprehensive fault bearing parameters are presented in Table 7. Vibration signals from the comprehen-sive fault bearing were acquired using the fault diagnosis test rig. Fig. 29 displays the acquired temporal waveform of the signal alongside the envelope spectrum derived from it, providing a visualization of the signal in the time and fre-quency domains.

Table 7. Combined-fault bearing parameters.

Parameter	Value
f_o (Hz)	90.25
f_b (Hz)	115.5
f_i (Hz)	135.75
Speed	1500RPM
Inner race defect (mm)	0.5 (width)
Ball defect(mm)	3 (Spalling)
Outer race defect(mm)	0.5 (width)

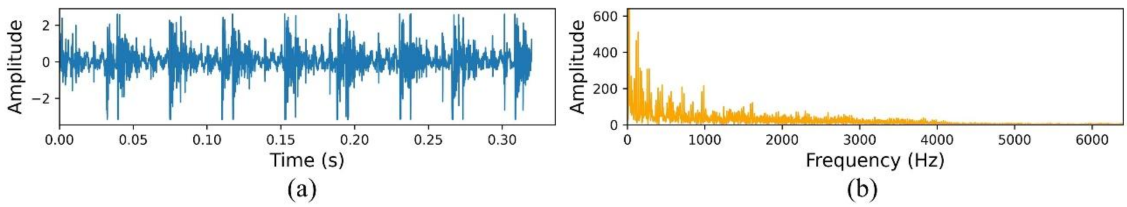

Figure 29. The (a)time domain waveform and (b)envelope spectrum of comprehensive fault bearing.

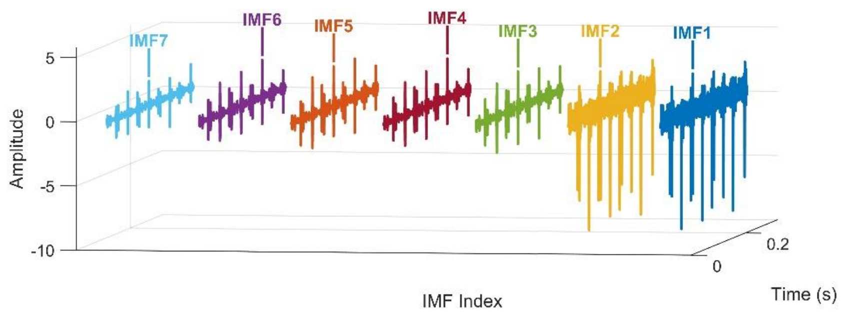

Figure 30. The processing result of EPFMD method to the comprehensive fault signal.

Similarly, the acquired comprehensive fault signal was first processed using the EPFMD method. The optimization procedure yielded an optimal parameter combination of filter length L = 60 and mode number n = 7. The resulting set of sub-modes from this decomposition is presented in Fig. 30 . The FEI was quantified for all derived sub-modes, with the results visualized in Fig. 31(a). IMF5, having the maxi-mum FEI value, was identified as the component for subse-quent envelope spectrum analysis. Fig. 31(b) displays the envelope spectrum obtained from the analysis of Case 2. To allow for clear differentiation among the potential fault sources pre-sent in the signal, a multi-color annotation scheme is em-ployed. The fundamental characteristic frequencies and their respective harmonics corresponding to the outer race, rolling element, and inner race defects are explicitly marked in red, violet, and green, respectively.

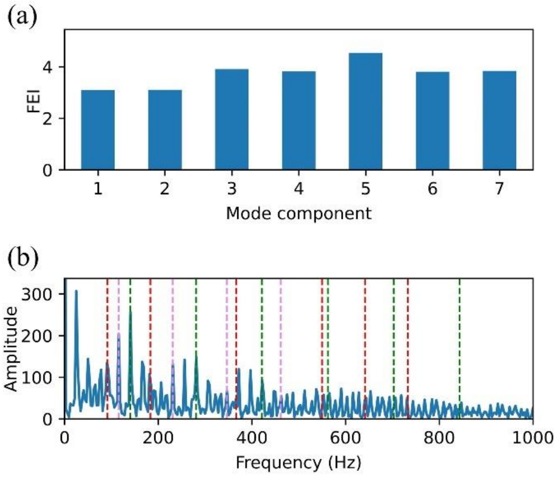

Figure 31. The EPFMD-based processing results (fo-red, fb-violet, fi-green): (a) FEI of each mode, (b) envelope spectrum of the dominant mode component.

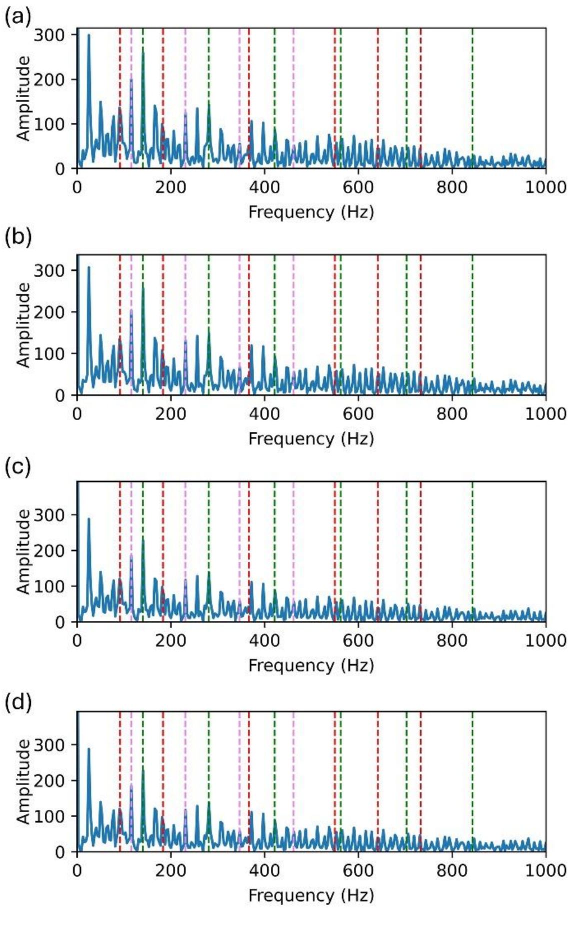

Figure 32. EPCHI is used as fitness function, and different optimization algorithms (a) COA, (b) SSA, (c) DBO and (d) ZOA are used to optimize FMD (fo-red, fb-violet, fi-green).

Fig. 31(b) clearly reveals the effective extraction of the characteristic frequencies for the rolling element (f_b), inner race (f_i), and outer race (f_o) faults. Additionally, their harmonic components ($2f_o$, $4f_o$, $6f_o$–$8f_o$; $2f_b$–$4f_b$; and $2f_i$–$6f_i$) are clearly identified. This provides evidence for the effectiveness of the proposed method in diagnosing comprehensive bearing faults.

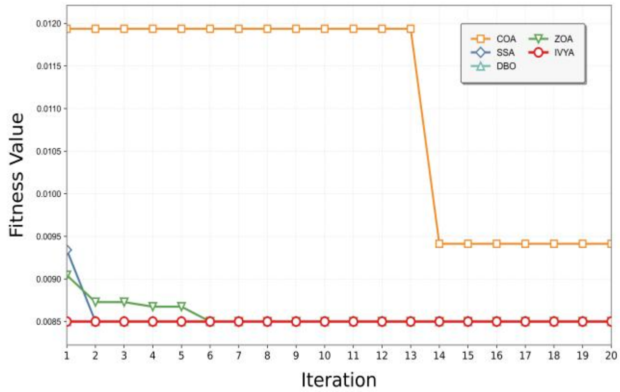

Figure 33. A comparison of the convergence characteristics of different optimization algorithms.

To validate the performance benefits of the proposed method, a comparative study was undertaken. Four distinct optimization algorithms—namely COA, SSA, DBO, and ZOA—were benchmarked by employing the EPCHI as the common fitness function. The FEI was computed for each of the decomposed sub-modes. And then the specific sub-mode characterized by the maximum FEI value was identi-fied as the most fault-sensitive component and selected for subsequent envelope analysis. Fig. 32 shows the results. All comparative methods reliably identified the characteristic frequencies associated with rolling element (fb), inner race (fi), and outer race (fo) faults and their corresponding harmonics, achieving a diagnostic performance on par with the IVYA-optimized FMD approach. The convergence curves of these algorithms (Fig. 33) show that IVYA and DBO exhibited the fastest convergence speeds for comprehensive fault diagno-sis.

Next, with IVYA fixed as the optimization algorithm, dif-ferent fitness functions (i.e. EE, PF, K, AEE and ESPF) were tested for FMD with adaptive parameter selection. The enve-lope spectra of the sub-modes with the highest FEI values were plotted separately, and the results are shown in the Fig. 34. Using EE as the fitness function, the fundamental fre-quencies (fo, fi, fb) and partial harmonics (2fo, 4fo, 6fo–8fo; 4fb–6fb; 2fi, 3fi) were extracted. However, fewer harmonics and lower amplitudes were observed for rolling element faults compared to EPFMD. For PF, K, and ESPF as fitness func-tions (Fig.

34(b), (c), and (e)), only limited harmonics (2fo, 4fo, 6fo; 2fb; 2fi–4fi) were resolved despite successful extraction of fundamental frequencies. When average envelope entropy (AEE) was used, even fewer harmonics (2fo, 4fo; 2fb; 2fi, 3fi) were identified. These results confirm the inferior perfor-mance of alternative fitness functions relative to EPFMD in diagnosing comprehensive bearing faults.

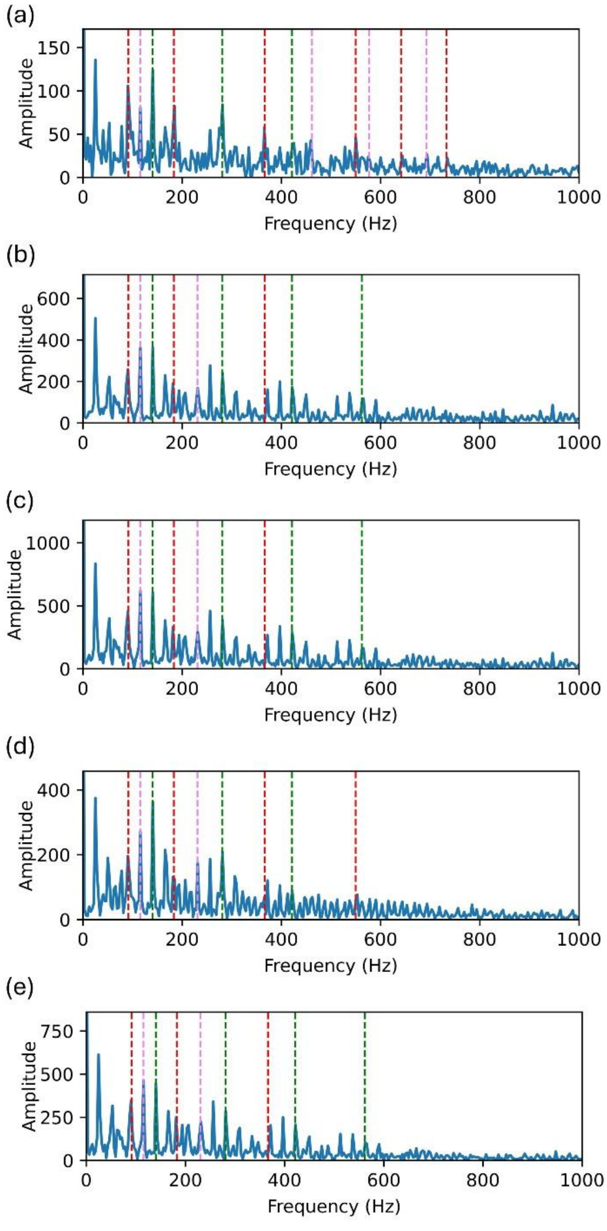

Figure 34. IVYA is used as optimization algorithm, and different fitness functions (a) EE, (b) PF, (c) K, (d) AEE and (e) ESPF are used to optimize FMD (fo-red, fb-violet, fi-green).

In order to further substantiate the effectiveness of the EPFMD method, a comparative analysis was performed against four established fault diagnosis techniques: IVYA-SVMD, IVYA-VMD, EWT, and SGMD. The comprehensive bearing fault signal was analyzed using each approach. The sub-mode with the highest FEI value from each technique was selected for envelope analysis, and Fig. 35 presents cor-responding results. For IVYA-SVMD (Fig.35(a)), all funda-mental frequencies (fo, fi, fb) were extracted, but only limited harmonics (2fo; 2fb; 2fi, 3fi) were extracted, significantly un-derperforming EPFMD. The IVYA-VMD method (Fig. 35(b)) successfully extracted the fundamental frequencies of all three bearing fault types (fo, fi, fb), but only identified the fifth and sixth harmonics （5fo, 6fo） of the outer race fault. Both the number and amplitude of the extracted harmonics were lower compared to the EPFMD method. EWT (Fig. 35(c)) extracted the fundamental frequencies along with 2fb and 2fi, but their harmonic counts and amplitude saliency were infe-rior to EPFMD. SGMD (Fig. 35(d)) identified the fundamental frequencies and three harmonics (2fb, 3fb, 3fi), but severe clutter interference sup-pressed both harmonic amplitudes and diagnostic reliability.

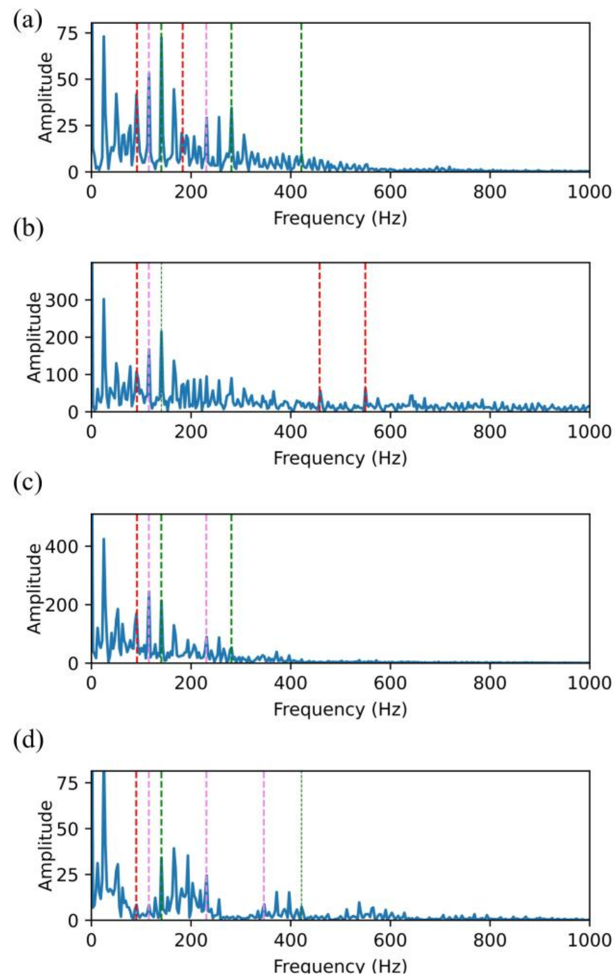

Figure 35. The (a) IVYA-SVMD, (b) IVYA-VMD, (c) EWT and (d) SGMD methods’results(fo-red, fb-violet, fi-green).

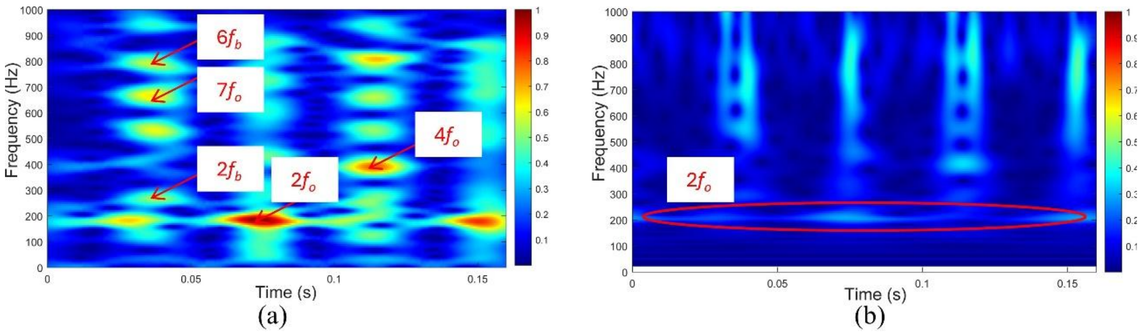

Figure 36. Processing results of two different time-frequency processing methods: (a) STFT, (b) GST.

For comparison, the capabilities of two time-frequency approaches (STFT and GST) was also analyzed, with the corresponding outcomes shown in Fig. 36. STFT (Fig. 36(a)) detected harmonics 2fo, 4fo, 7fo, 2fi, and 6fi, but failed to resolve any fundamental frequencies or inner race fault components. GST (Fig. 36(b)) extracted only 2fo, demonstrating negligible diagnostic utility for comprehensive faults.

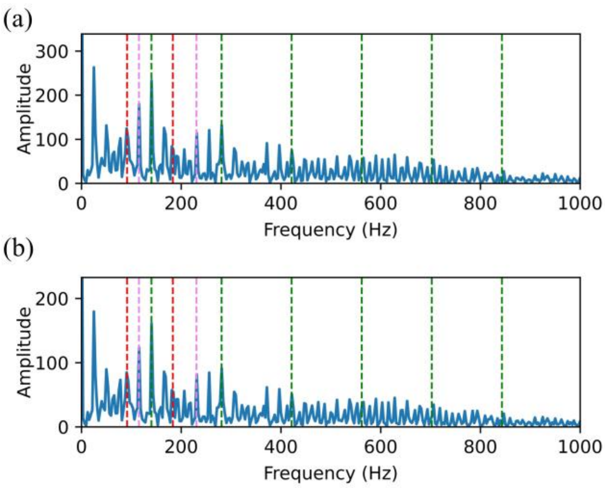

Figure 37. The (a) POFMD and (b) AHA-FMD methods' results (fo-red, fb-violet, fi-green).

The comprehensive fault signal of bearings was further processed using the two aforementioned improved FMD methods. Envelope analysis was performed on the sub-mode with the maximum FEI value. The results, presented in Figs. 37(a) and (b), show that POFMD effectively extracted the fault characteristic frequencies of the outer race (f_o), ball (f_b), and inner race (f_i), in addition to their respective harmonics ($2f_o$; $2f_b$; $2f_i$-$6f_i$), as evidenced in Fig. 37(a). However, the number of extracted harmonics remains inferior to the EPFMD method. Similarly, the results from AHA-FMD in Fig. 37(b) confirm the method's effectiveness by clearly revealing the characteristic frequencies (f_o, f_b, f_i) and their harmonics ($2f_o$; $2f_b$; $2f_i$-$6f_i$). Nevertheless, both amplitude significance and harmonic quantity are inferior to the proposed method.

Through Case 2 comparative analysis, the superiority of EPFMD in diagnosing comprehensive rolling bearing faults is conclusively established.

5.2.3. Quantitative comparative analysis

The superiority and effectiveness of the EPFMD method in diagnosing rolling bearing faults have been validated through a series of longitudinal and horizontal experimental studies involving dataset analysis and case studies. However, these conclusions remain qualitative. A comprehensive quantitative evaluation was conducted to provide a holistic assessment of the method's performance. Four critical metrics—the FEI, kurtosis, the EPCHI, and computational time—were benchmarked across all tested methodologies. The comparative results, systematically summarized in Fig. 38. In Fig. 38(a), EPFMD achieves higher FEI values than other methods for the CWRU dataset and both test rig cases, except in Case 1. It should be noted that the FEI primarily reflects the impulsiveness and spectral concentration characteristics of the extracted signal, rather than directly representing the final fault identification accuracy. In some cases, excessively enhanced impulse noise or interference components may lead to higher FEI values. Therefore, a larger FEI does not necessarily indicate better fault diagnosis performance. Compared with other methods, the proposed approach can more effectively preserve the inherent periodic fault structure, extract clearer fault characteristic frequencies, and thereby obtain more reliable fault identification results. Despite not having the highest FEI value in Case 1, EPFMD demonstrates superior fault identification accuracy (see Fig.11, 12, 14, 15 and 17), quantitatively confirming its exceptional defect extraction capability. Analysis of the CWRU dataset results in Fig. 38(b) indicates minimal variation in the kurtosis values across all 16 diagnostic methods, underscoring this metric's limited sensitivity to fault-induced impulses under strong background noise. In contrast, for the experimental test rig cases, the five methods utilizing the composite health indicator EPCHI as the fitness function—namely, EPFMD, COA-EPCHI, SSA-EPCHI, DBO-EPCHI, and ZOA-EPCHI—consistently demonstrate superior performance. This is evidenced by their significantly higher Fusion Evaluation Index (FEI) and kurtosis values compared to both the methods using alternative fitness functions (IVYA-EE, IVYA-PF, etc.) and the benchmark improved FMD approaches (POFMD, AHA-FMD), quantitatively proving EPCHI's superior sensitivity to bearing fault characteristics. As can be observed from Fig. 38(c), EPFMD achieves lower EPCHI values than other methods except for IVYA-FMD on the CWRU dataset and SGMD in Case 2, highlighting its advantage in fault feature extraction. Comparative analysis of Fig. 38(b) and (c) demonstrates that the proposed EPCHI exhibits greater sensitivity to defect-induced transients and stronger noise robustness than kurtosis, further validating its effectiveness in evaluating fault signal sparsity and impulsivity. Practical fault diagnosis requires not only accuracy but also efficiency for timely troubleshooting. Computational time was evaluated across methods (Fig. 38(d)). While non-adaptive signal processing methods, including IVYA-VMD, EWT, and SGMD, are characterized by their shorter computational runtimes, their diagnostic utility is significantly limited by a comparatively poor sensitivity to transient fault features, as evidenced in Figs. 15, 26, and 35. Within adaptive methods, EPFMD achieves competitive computational efficiency while maintaining diagnostic accuracy, attaining an optimal balance. Concurrently, compared with improved FMD methods, EPFMD demonstrates demonstrates measurable advantages in operational efficiency. Ultimately, quantitative analysis across four metrics firmly establishes EPFMD's advantages in applications of rolling bearing defect detection.

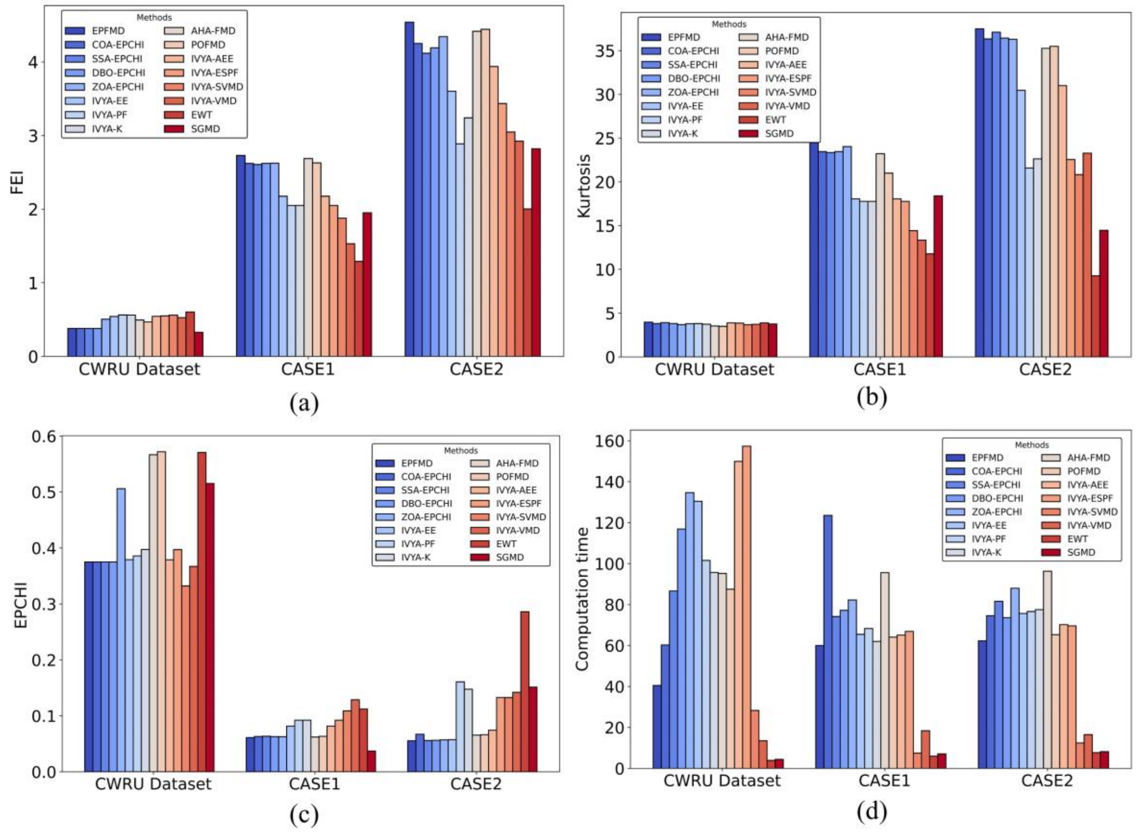

Figure 38. Quantitative indicators for different methods.

6. Conclusion

Focusing on the difficulty of extracting fault features under strong background noise, the present work develops a parameter-adaptive FMD method. The approach is capable of automatic adaptation to bearing vibration signal characteristics, performing accurate fault diagnosis in mechanical systems under complex conditions. By dynamically optimizing key parameters during the decomposition process, an autonomous parameter optimization mechanism is established. This approach effectively addresses critical limitations of traditional FMD methods which are caused by manual parameter presetting. We experimentally verified the method on public bearing datasets and the PT870 test rig system. Results illustrate that the method retains stable diagnostic capabilities under complex scenarios, including strong noise interference and comprehensive faults. Through vertical comparisons (e.g., COA-EPCHI, IVYA-EE, IVYA-PF), horizontal comparisons (e.g., IVYA-VMD, EWT), and benchmarking against improved FMD methods, the proposed approach demonstrates significant advantages in key metrics such as fault feature identifiability and computational efficiency. Our primary innovations are as follows:

This study proposes an innovative rolling bearing fault diagnosis approach. A novel composite health indicator, termed EPCHI, is constructed by integrating envelope en-tropy (EE) with the pulse factor (PF). This integration is designed to concurrently characterize two critical proper-ties of fault signals: sparsity, as measured by EE, and im-pulsiveness, as quantified by PF. A comparative evalua-tion demonstrates that the composite health indicator EPCHI achieves superior performance in both fault fea-ture characterization and noise robustness when bench-marked against conventional indicators, including EE, PF, Kurtosis, AEE, and ESPF. Utilizing EPCHI as the fitness function, the IVYA algorithm optimizes parameters for FMD, establishing a parameter-adaptive FMD diagnostic framework. This synergizes IVYA's global optimization capability with FMD's decomposition performance, ena-bling precise fault diagnosis without prior knowledge. By integrating kurtosis (capturing transient impacts in fault signals) and spectral entropy (characterizing periodic fea-tures of fault signals), the fusion evaluation index (FEI) is constructed as the criterion for dominant mode selection. Through qualitative analysis and quantitative comparison across multi-dimensional metrics, the dual superiority of the approach in diagnostic accuracy and efficiency is ver-ified.

Although the proposed method achieved satisfactory di-agnostic performance under the experimental conditions investigated in this study, the validation data were obtained from a single bearing fault simulation platform. Therefore, the generalization capability of the proposed method under more complex industrial environments still requires further investigation. In practical engineering applications, factors such as variable speed, load fluctuations, structural coupling, and compound faults may influence the robustness of the method. Future work will focus on conducting cross-platform experiments and field validations using real industrial data to further evaluate the practical applicability and engineering reliability of the proposed framework.

Acknowledgment

This work was financially supported by the National Sci-ence Foun dation for Distinguished Young Scholars of China (Grant No.52402522) and Shanxi Key Laboratory of High-end Equipment Reliability Tech nology (No.446110103). The authors would like to express their grati tude to the edi-tors and anonymous reviewers for their valuable suggestions.

References

1. Zhong H, He D, Sun H, He C, Lao Z. A novel meta-learning method based on relation network for train bearing fault diagnosis. *Nonlinear Dynamics* 2025; 113: 27001-29. https://doi.org/10.1007/s11071-025-11555-9.
2. Guo J, Wang S, Guan W, Wang G, Liu Z, Wu S. Research on noise-robust fault diagnosis method for rotating machinery in dynamic environments based on multi-scale convolution. *Nonlinear Dynamics* 2025; 113: 33399-421. https://doi.org/10.1007/s11071-025-11722-y.
3. Zhuang Y, He D, Jin Z, Wei Z, Sun H, Wu J, et al. SWR2 Net: a fault diagnosis framework for rotating machine under limited samples and noise interference. *Nonlinear Dynamics* 2025; 113: 22823-52. https://doi.org/10.1007/s11071-025-11302-0.
4. Dong Y, Jiang H, Wang X, Li Z. Entropy-Oriented Semi-Supervised Dynamic Prototype Contrastive Learning for Rotating Machinery Fault Diagnosis. *IEEE/ASME Transactions on Mechatronics* 2025; 30: 4934-45. https://doi.org/10.1109/TMECH.2025.3570186.
5. Wang X, Jiang H, Dong Y, Mu M. Spatial-channel collaborative multi-scale graph interaction deep transfer learning for unsupervised rotating machinery fault diagnosis. *Engineering Applications of Artificial Intelligence* 2026; 176: 114691. https://doi.org/10.1016/j.engappai.2026.114691.

6. Li Z, Jiang H, Dong Y. A convolutional-transformer reinforcement learning agent for rotating machinery fault diagnosis. *Expert Systems with Applications* 2025; 271: 126669. https://doi.org/10.1016/j.eswa.2025.126669.
7. Yan J, Zhu X, Wang X, Zhang D. A New Fault Diagnosis Method for Rolling Bearings with the Basis of Swin Trans-former and Generalized S Transform. *Mathematics* 2024; 13: 45. https://doi.org/10.3390/math13010045.
8. Hou J, Wu Y, Ahmad AS, Gong H, Liu L. A Novel Rolling Bearing Fault Diagnosis Method Based on Adaptive Feature Selection and Clustering. *IEEE Access* 2021; 9: 99756-67. https://doi.org/10.1109/ACCESS.2021.3096723.
9. Yan X, Liu Y, Jia M. A Fault Diagnosis Approach for Rolling Bearing Integrated SGMD, IMSDE and Multiclass Relevance Vector Machine. *Sensors* 2020; 20: 4352. https://doi.org/10.3390/s20154352.
10. Chennana A, Ahmia A, Megherbi AC, Bessous N, Sbaa S, Teta A. A Bearing Faults Diagnosis Enhancement Using EMD and MEDA. *2024 2nd International Conference on Elec-trical Engineering and Automatic Control (ICEEAC)*, Setif, Al-geria: IEEE; 2024, p. 1–6. https://doi.org/10.1109/ICEEAC61226.2024.10576278.
11. Xu L, Li W, Zhang B, Zhu Y, Lang C. Fault Diagnosis of Mine Truck Hub Drive System Based on LMD Multi-Component Sample Entropy Fusion and LS-SVM. *Actuators* 2023; 12: 468. https://doi.org/10.3390/act12120468.
12. Liu F, Wang H, Li W, Zhang F, Zhang L, Jiang M, et al. Fault diagnosis of rolling bearing combining improved AWSGMD-CP and ACO-ELM model. *Measurement* 2023; 209: 112531. https://doi.org/10.1016/j.measurement.2023.112531.
13. Chauhan S, Vashishtha G, Kumar R, Zimroz R, Gupta MK, Kundu P. An adaptive feature mode decomposition based on a novel health indicator for bearing fault diagnosis. *Measurement* 2024; 226: 114191. https://doi.org/10.1016/j.measurement.2024.114191.
14. Wang S, Xiang J, Tang H, Liu X, Zhong Y. Minimum entropy deconvolution based on simulation-determined band pass filter to detect faults in axial piston pump bearings. *ISA Transactions* 2019; 88: 186-98. https://doi.org/10.1016/j.isatra.2018.11.040.
15. Guo J, Liu Y, Yang R, Sun W, Xiang J. A simulation-driven difference mode decomposition method for fault diagnosis in axial piston pumps. *Advanced Engineering Informatics* 2024; 62: 102624. https://doi.org/10.1016/j.aei.2024.102624.
16. Li J, Wang Y, Xiang J, Chen Z. A simulation guided BCSM blind deconvolution for fault diagnosis in wind turbine bearing. *Measurement Science and Technology* 2025; 36: 036143. https://doi.org/10.1088/1361-6501/adb6c6.
17. Li J, Liu Y, Chen Q, Xiang J. Simulation-driven bandpass filter in association with an optimal bandwidth to detect faults in axial piston pumps. *Measurement Science and Technology* 2023; 34: 095116. https://doi.org/10.1088/1361-6501/acdc42.
18. Miao Y, Zhang B, Li C, Lin J, Zhang D. Feature Mode Decom-position: New Decomposition Theory for Rotating Machinery Fault Diagnosis. *IEEE Trans Ind Electron* 2023; 70: 1949-60. https://doi.org/10.1109/TIE.2022.3156156.
19. Garcés MA. Quantized Information in Spectral Cyberspace. *Entropy* 2023; 25: 419. https://doi.org/10.3390/e25030419.
20. Wang B, Tang H, Zu X, Chen P. Adaptive Feature Extraction Using Sparrow Search Algorithm-Variational Mode Decom-position for Low-Speed Bearing Fault Diagnosis. *Sensors* 2024; 24: 6801. https://doi.org/10.3390/s24216801.
21. Ghasemi M, Zare M, Trojovský P, Rao RV, Trojovská E, Kan-dasamy V. Optimization based on the smart behavior of plants with its engineering applications: Ivy algorithm. *Knowledge-Based Systems* 2024; 295: 111850. https://doi.org/10.1016/j.knosys.2024.111850.
22. Wei D, Jiang H, Shao H, Li X, Lin Y. An optimal variational mode decomposition for rolling bearing fault feature ex-traction. *Measurement Science and Technology* 2019; 30: 055004. https://doi.org/10.1088/1361-6501/ab0352.
23. Lu JT, Yao T, Li SM, Cui RQ. An intelligent fault diagnosis method for rolling bearings based on hybrid characteristics. *Journal of Vibration and Shock* 2022; 41: 79-84. https://doi.org/10.13465/j.cnki.jvs.2022.16.011.
24. Yan X, Jia M. Bearing fault diagnosis via a parameter-optimized feature mode decomposition. *Measurement* 2022; 203: 112016. https://doi.org/10.1016/j.measurement.2022.112016.
25. Sun Y, Cui J. Rolling bearing fault diagnosis: a parameter adaptive method based on a new fitness function. *Results in Engineering* 2025; 28: 107224. https://doi.org/10.1016/j.rineng.2025.107224.
26. Case western reserve university bearing data center web-site n.d.